Proceedings Paper:

Rodriguez Lago, P. orcid.org/0000-0003-1979-4018, Nutter, J., Qi, J. orcid.org/0000-0001-5235-0027 et al. (2 more authors) (2023) Characterisation of the wear and friction behaviour of laser deposited cobalt and iron-based hardfacing alloys for nuclear applications. In: Hanke, S., (ed.) Wear. 24th International Conference on Wear of Materials, 16-20 Apr 2023, Banff, Canada. Elsevier BV. Article no: 204829. ISSN: 0043-1648. EISSN: 1873-2577.

https://doi.org/10.1016/j.wear.2023.204829

Wear 524-525 (2023) 204829

Contents lists available at ScienceDirect

Wear

journal homepage: www.elsevier.com/locate/wear

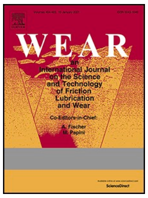

Characterisation of the wear and friction behaviour of laser deposited cobalt and iron-based hardfacing alloys for nuclear applications

P. Rodriguez Lago [a], J. Nutter [a], J. Qi [a], D. Stewart [b], W.M. Rainforth [a,*]

[a] Department of Material Science and Engineering, The University of Sheffield, Mappin Street, Sheffield, S1 3JD, UK
[b] Rolls-Royce plc, Derby, DE24 8BJ, UK

ABSTRACT

Valves and pumps in nuclear plants operate in a particularly aggressive environment of a high neutron flux, high contact loads and in superheated water up to 300 °C. Traditionally there has only been one material that can survive these conditions: cobalt based hardfacing alloys called Stellites. There is an urgent need to replace cobalt-based alloys because of the formation of cobalt-60 radioisotope, which causes radioactive exposure. In this study an iron-based hardfacing alloy, Tristelle 5183 was compared with Stellite 6. The hardfacings were manufactured via laser cladding. Wear testing was performed using a pin-on-flat configuration, with like-on-like couples, from room temperature up to 300 °C with loads of 50–500 N. The friction coefficient for the Tristelle was higher (typically 0.45) than the Stellite (typically 0.35) across all temperatures and loads. The wear rate of the Tristelle was higher than the Stellite, but the exact difference varied with both load and temperature. The specific wear rate increased with temperature, but only gradually. The operative wear mechanism was a combination of adhesive and oxidational wear, but there were significant differences found between the two alloys. For the Tristelle, the oxide became mechanically mixed with the heavily deformed surface metal. In contrast, the oxide on the Stellite was detached from the surface without any mechanical mixing. The extent of surface deformation was much greater for the Tristelle than the Stellite. The large (5–20 mm) NbC in the Tristelle fractured a considerable distance (up to 40 mm) below the worn surface and became increasingly fine as the worn surface was approached as a result of high strain deformation in the matrix. In the Stellite no carbide fracture was observed. The reasons for the marked difference in behaviour between the two alloys, each with the same mechanical properties, are discussed in detail.

1. Introduction

Nuclear power plants are complex engineering structures with a multitude of different components required to make them operate. Much is made of key components, such as the pressure vessel. One area that rarely hits the headlines, but is fundamental to the operation of the plant, is tribological components such as valves and pumps. These components operate in a particularly aggressive environment; the materials are subjected to a neutron flux, to high load contact and relative motion. Unlike, for example, an internal combustion engine where lubrication is provided by highly optimised oils, in a nuclear power plant the lubricant is just superheated water.

Traditionally, there has only been one material that can survive this highly hostile environment: cobalt based Stellite hard facing alloys. However, there is a big problem with cobalt-based alloys. The exposure of cobalt to a neutron flux results in the formation of cobalt-60 radioisotope, which is one of the principal root causes of the dose received by site workers and also contributes to radioactive waste [1]. The obvious answer to this problem is to remove the cobalt from the hard facing. The next generation of nuclear power plants will therefore require new alloys to replace the traditionally used cobalt-based hard facings. These alloys will have to be iron based in order to ensure low activation. The replacement alloys must meet the performance standards set by Stellite, specifically they must resist galling and exhibit very low sliding wear rates, both at elevated temperature.

There are several important components to the material's microstructure which are key to make it successful for this application and be resistant to both galling and sliding wear. Firstly, the alloy must have excellent corrosion and oxidation resistance which is usually imparted by the addition of chromium. Thus, the alloys are based on a stainless steel. Secondly, the alloy must have a matrix that is highly resistant to plastic deformation, which requires a low stacking fault energy; galling resistance is widely believed to scale with a reduction in stacking fault energy [2]. Thirdly, the alloy must contain a uniform dispersion of hard, tough, second phase particles that provide load support. Overall, the alloy must have good thermal conductivity. The iron-based alloys are based on a stainless steel matrix, often austenitic, but also ferritic or a mixture of the two phases. They contain a large volume fraction of hard carbides and possibly silicides.

There has been extensive work on iron-based alternatives to Stellite

---

* Corresponding author.
E-mail address: m.rainforth@sheffield.ac.uk (W.M. Rainforth).

https://doi.org/10.1016/j.wear.2023.204829
Received 15 September 2022; Received in revised form 23 January 2023; Accepted 25 January 2023

Table 1
The chemical composition of Stellite 6, Tristelle 5183 and NOREM 02 as provided by the supplier.

Alloy	Element (wt%)								
	Fe	Cr	Ni	Si	C	Nb	Co	Mn	Others
Stellite 6	1.3	27.5	2.6	–	1.1	–	Bal.	0.25	4.2W
Tristelle 5183	Bal.	20.0	10.0	4.0	2.0	8.0	–	–	–
NOREM 02	Bal.	25.0	4.0	3.3	1.2	–	–	4.5	2.0Mo

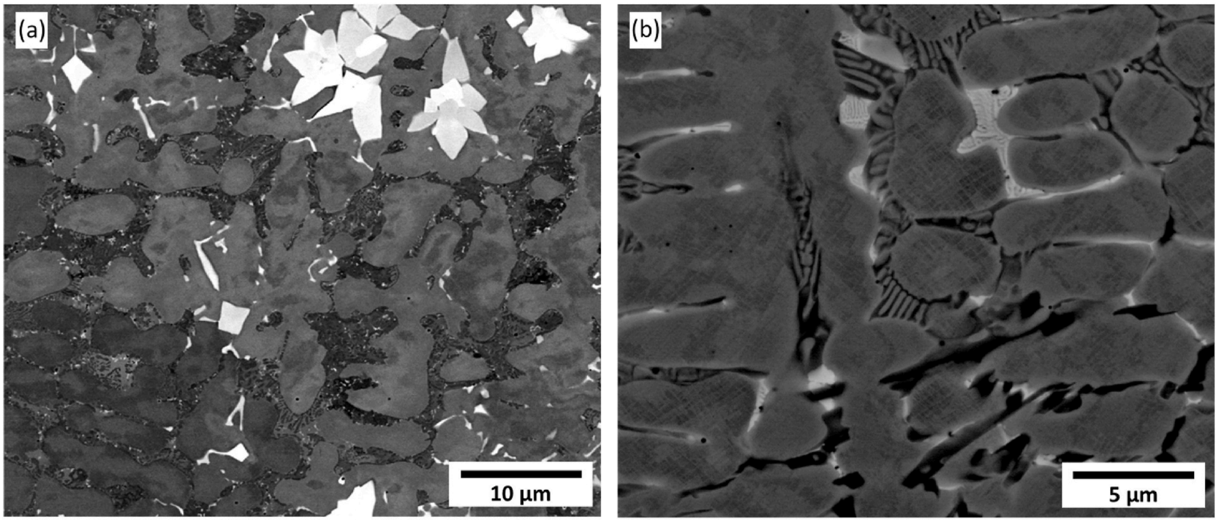

Fig. 1. Back scattered electron images showing the microstructure of the as-deposited materials. a) Tristelle 5183 cladding, showing the matrix, M_7C_3 and niobium carbides (bright contrast). b) the matrix, M_7C_3 (dark contrast) and regions rich in W and Si (bright contrast).

[3–12]. In the early 90's, Burdett evaluated different types of alloys for galling resistance, corrosion and weldability. The galling tests were in a pin-on-disk configuration, with the load increased until galling was observed. Burdett [3] reported that some iron-based alloys (Delcrome 910 and Tristelle 5183) showed promising results on the corrosion as well as the galling tests, even at 300 °C. Shiels et al. [4] further analysed the most significant iron-based alloys that performed well in previous studies [3,5]. The reciprocating flat-on-flat wear tests results were similar to those observed before [3,6] and most alloys showed similar or even better results than Stellite 6. Recently, Smith et al. [2] have shown that Nitromaxx, a Fe-based hard facing alloy exhibits galling resistance comparable to Stellite 6 up to 350 °C. The success of Nitromaxx was attributed to reducing the stacking fault energy of the matrix through nitrogen additions, which suppresses strain localisation, which is considered to be the origin of galling. Kim and Kim [7] looked at another alternative iron-based alloy, NOREM, which was found to gall at temperatures higher than 180 °C. The transition to severe adhesive wear that took place was explained by Kim and Kim based on the loss of the work-hardening ability of the NOREM 2 due to an increase of the stacking fault energy (SFE) derived from the rise in temperature, which also reduces the formation of strain induced martensite, which is considered to produce an increase in wear resistance. However, below 180 °C the NOREM 2 provided wear resistance that matched the Stellite, attributed to the beneficial effects of the oxide that formed on the surface.

The alloy development has focused extensively on the galling resistance of the Fe-based hard facing materials compared to Stellite. This has been driven by a need to reduce the stacking fault energy of the matrix to improve the resistance to strain localisation and hence improve galling resistance. However, the alloys have to also provide excellent sliding wear resistance. The microstructural requirements for sliding wear resistance are not the same as galling, with other factors such as hard, tough second phases and the corrosion resistance becoming very important. In this study, an iron-based hard facing, Tristelle 5183 is compared to the standard cobalt-based alloy, Stellite 6 under dry sliding conditions. A detailed analysis of the friction and wear behaviour from room temperature up to 300 °C is presented. Particular attention is paid to try and understand the fundamental differences between a cobalt-based matrix and an iron-based matrix.

2. Experimental

2.1. Materials

The starting materials used for this study were a cobalt-based superalloy, Stellite 6, and an iron-based alloy, Tristelle 5183. The composition of each alloy is shown in Table 1. The materials were manufactured by firstly producing a powder of the alloy followed by laser deposition. The gas-atomised powder of the 60–150 μm mesh size was supplied by LSN Diffusion, UK. Laser cladding was undertaken at LASE LTD, UK, using 100 × 100 × 20 mm 316L stainless steel substrates (supplied by Nationwide Stainless LTD, UK). A substantial number of runs were conducted to optimise the deposition conditions.

2.2. Wear testing

The pins for the reciprocating wear tests were machined from the welded plates via electro discharge machining (EDM) at Ian Cocker Precision Engineering, UK. The pins were cylindrical with a total length of 22 mm and a diameter of 6.2 mm on one end and 3 mm on the contact end. Disc specimens, approximately 15 × 15 × 3mm, were also removed from the laser clad material by EDM. Pin and disc specimens were prepared to a high metallographic finish using standard grinding and polishing techniques to create a flat like-on-like contact.

A Bruker UMT Tribolab machine was used to perform the wear tests using a reciprocating pin-on-flat configuration, which is similar to the work carried out by Kim and Kim [7]. Loads were chosen to give Hertzian contact stresses in the range experienced by a hardfacing in a pump

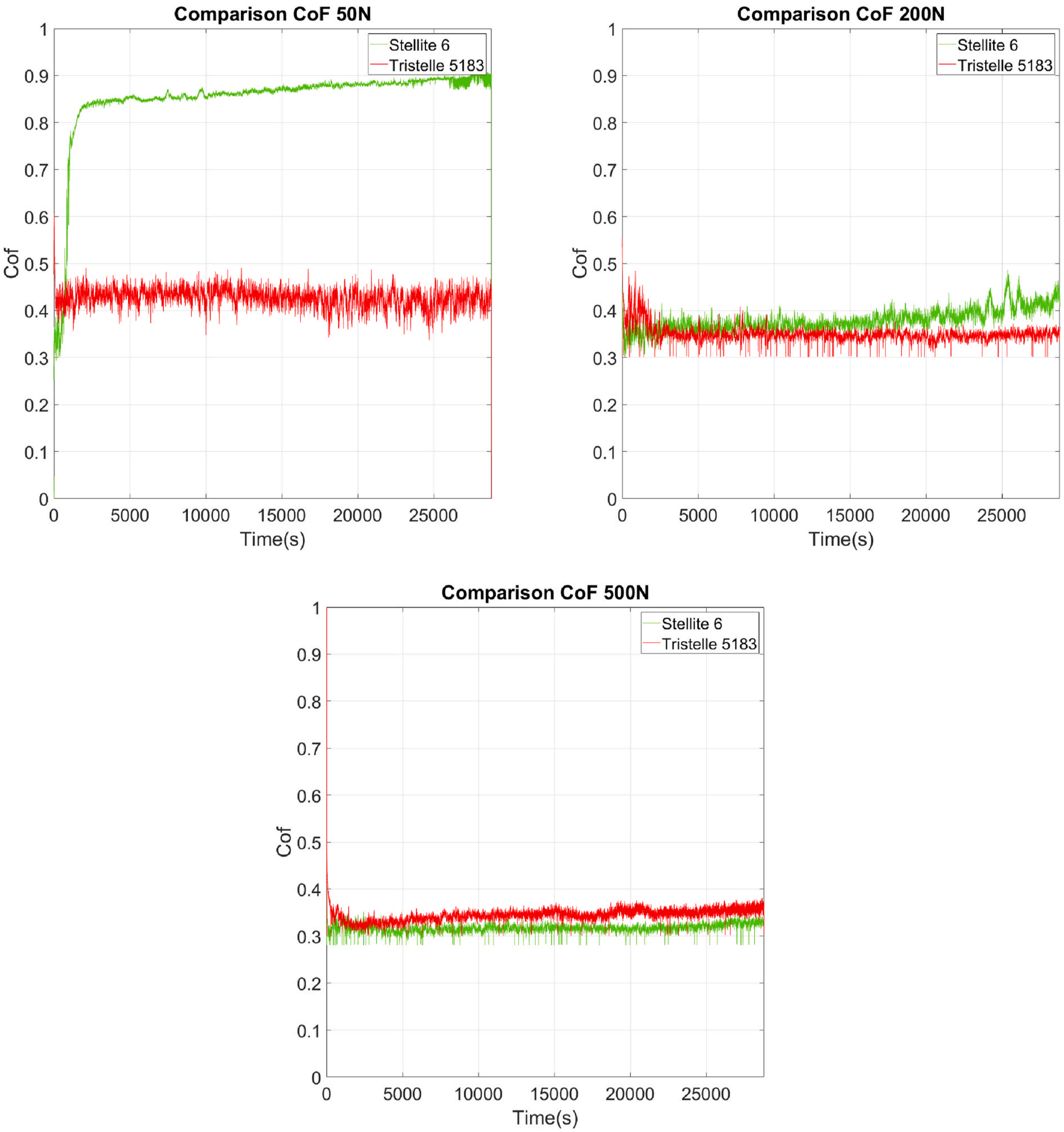

Fig. 2. Friction coefficient as a function of test time at room temperature for 50, 200 and 500 N.

application. However, the loads chosen were intentionally below the values that would be expected to give galling since we wished to avoid galling in these particular tests. Therefore, a load of 50 N was selected for the initial tests, with a 9 mm stroke length at a speed of 3 mm per second for 100 cycles. Following this, room temperature tests were performed at 50 N, 200 N and 500 N at this sliding speed and stroke length. Assuming a flat-on-flat configuration with 3 mm diameter round contact, the Hertzian contact pressures were calculated as 7.1 MPa, 28.3 MPa and 70.7 MPa for 50 N, 200 N and 500 N respectively. The reciprocating tests ran for 8h hours each in order to produce sufficient wear and study the differences between the alloys, giving a total sliding distance of 86.4 m per test. The laser deposition produces an as-cast microstructure with a strong columnar structure. Therefore, all pins were slid against the disk diagonally in relation to this strongly textured structure in order to obtain a better representation of the wear characteristics of each alloy.

The effect of temperature was studied using temperatures of 100 °C, 200 °C and 300 °C. A 30-min window was left before each test to stabilize the temperature once it was reached. Loads of 50 N and 200 N were used, but a load of 500 N was not possible because of the limitations of the test rig. The sliding speed and distance were the same as for the room temperature tests.

The coefficient of friction data was recorded by the UMT software by measuring the tangential force during the tests. To avoid excessive noise and remove the zero values when the pin reaches each side of the wear track, the friction was taken as that in the middle of each stroke. The 50 N test at room temperature was run twice to establish the repeatability of the tests and the results were acceptable.

2.3. *Characterisation*

A Durascan hardness testing machine was utilized to measure the

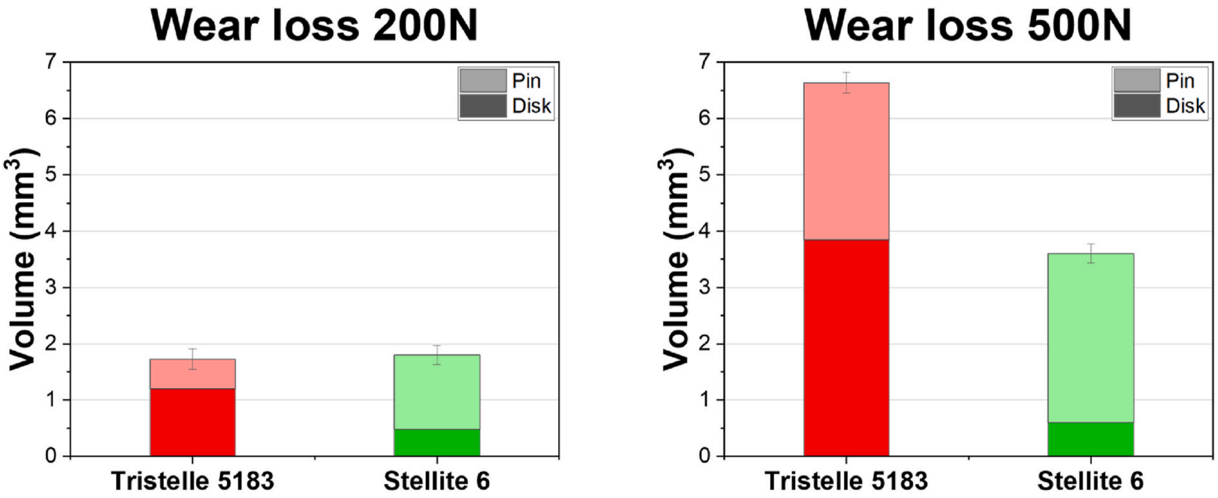

Fig. 3. Volume wear loss for the materials tested at room temperature for 200 and 500 N.

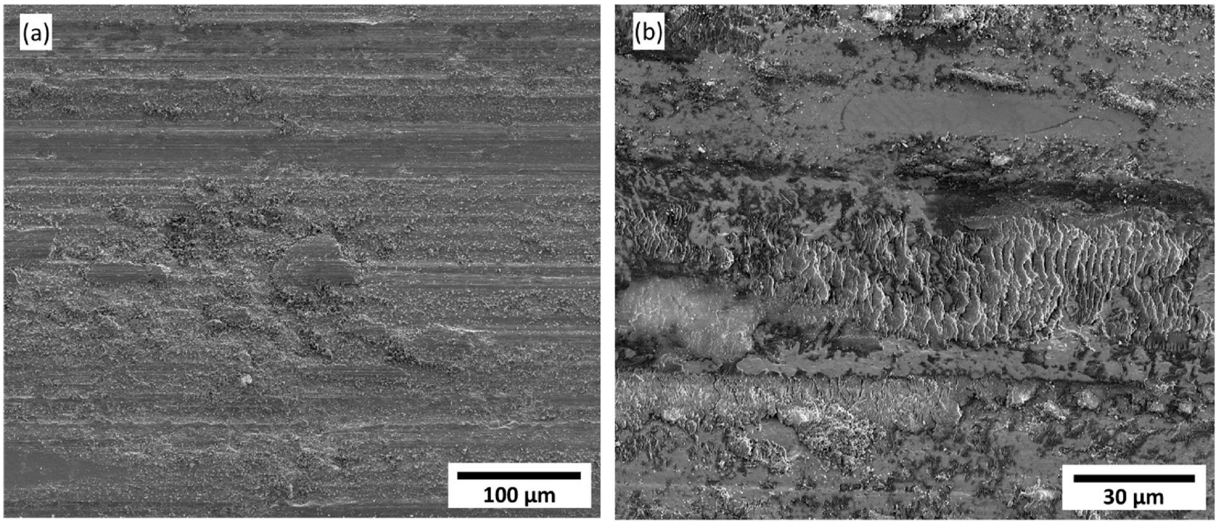

Fig. 4. Secondary electron SEM images after the room temperature tests at 50 N. a) Tristelle, b) Stellite.

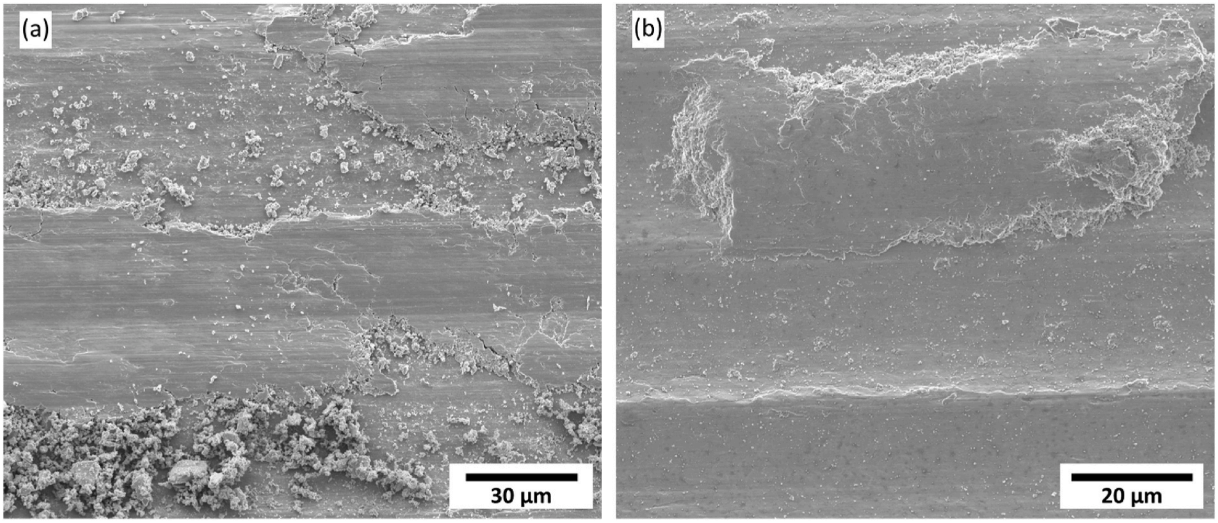

Fig. 5. Secondary electron SEM images after the room temperature tests at 200 N. a) Tristelle, b) Stellite.

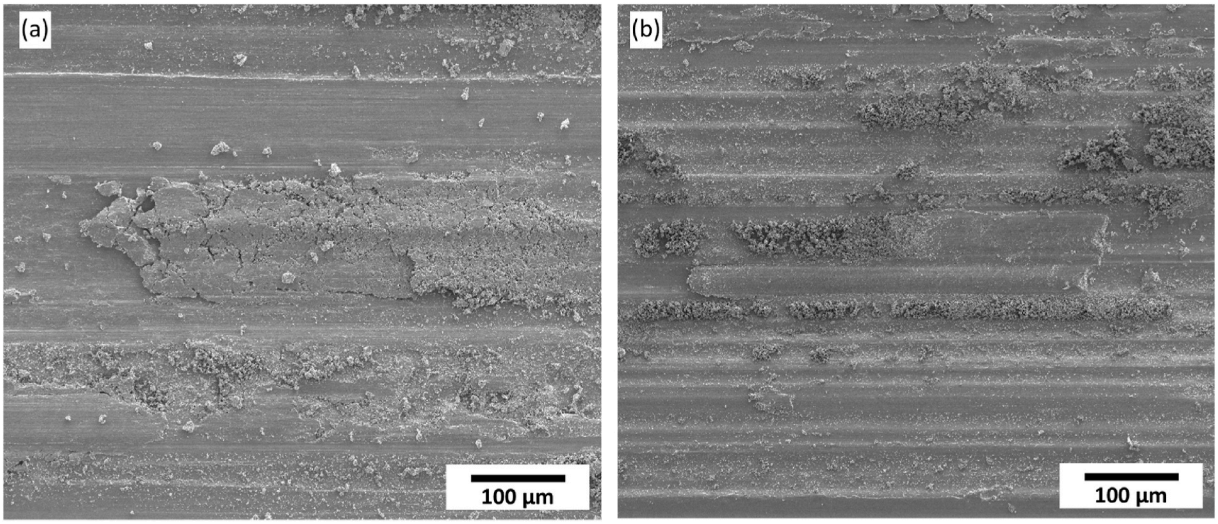

Fig. 6. Secondary electron SEM images after the room temperature tests at 500 N. a) Tristelle, b) Stellite.

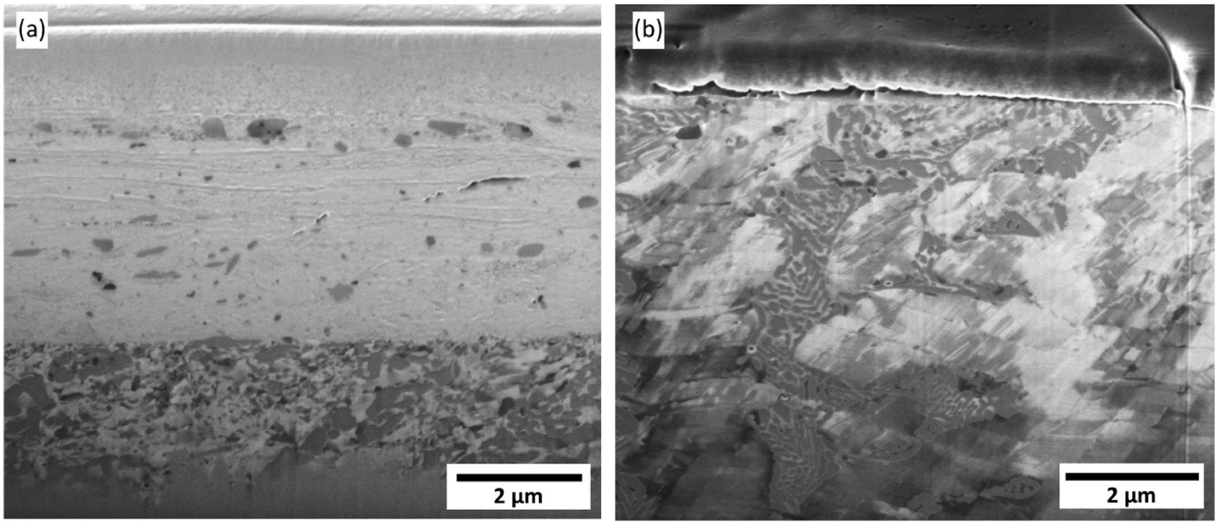

Fig. 7. Ion channelling images from FIB cross-sections of the discs after testing at 50 N at room temperature, a) Tristelle, b) Stellite.

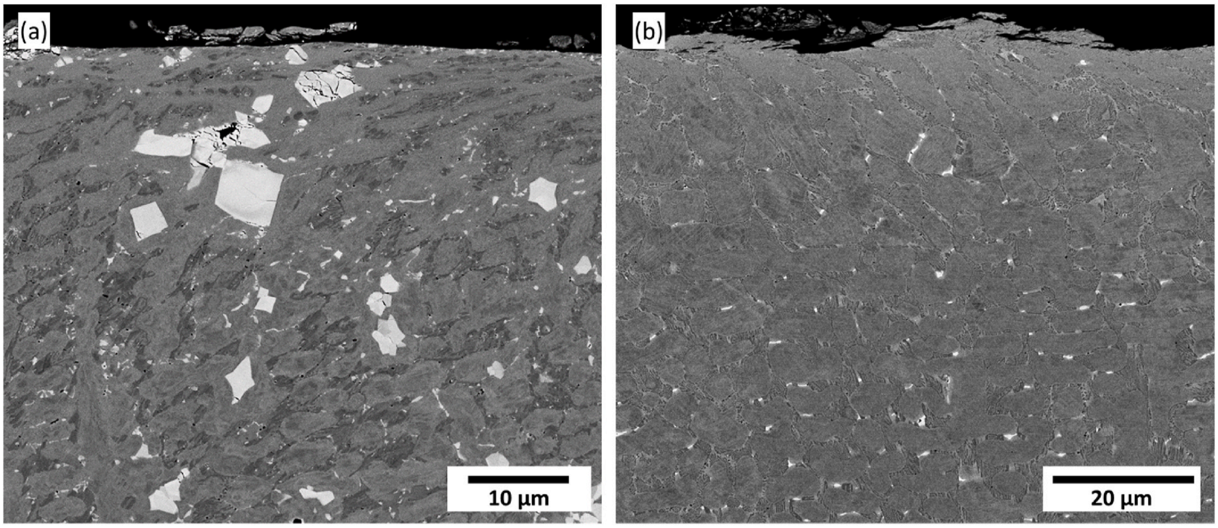

Fig. 8. Backscattered electron images of cross-sections of (a) Tristelle 5183 (b) Stellite 6 pins after the 500 N sliding wear tests at room temperature.

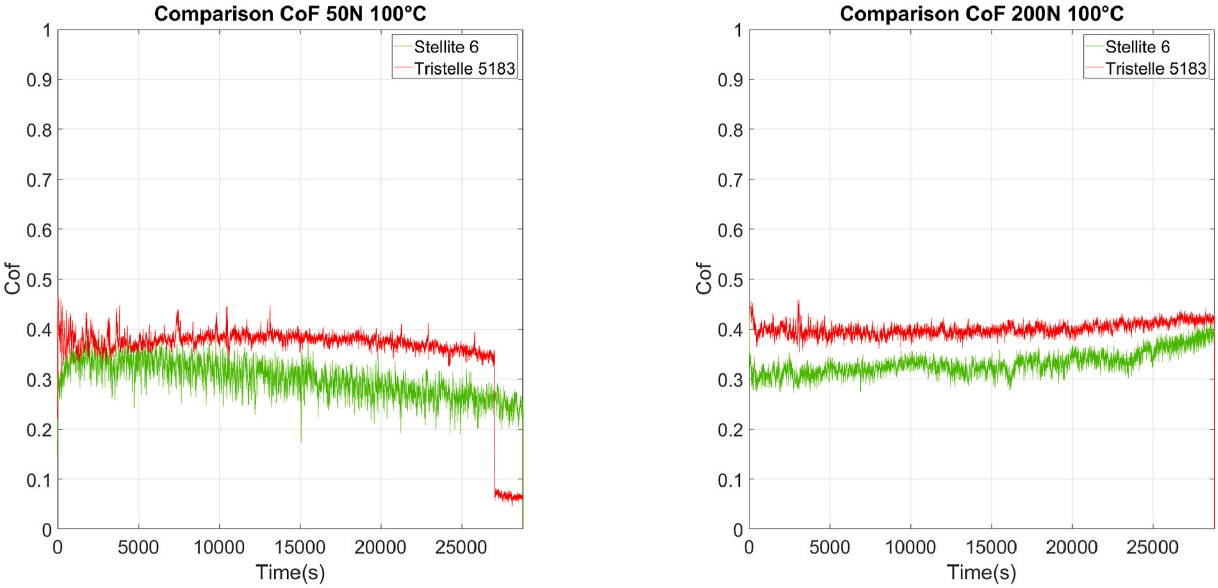

Fig. 9. Friction behaviour of the materials at 100 °C at 50 and 200 N.

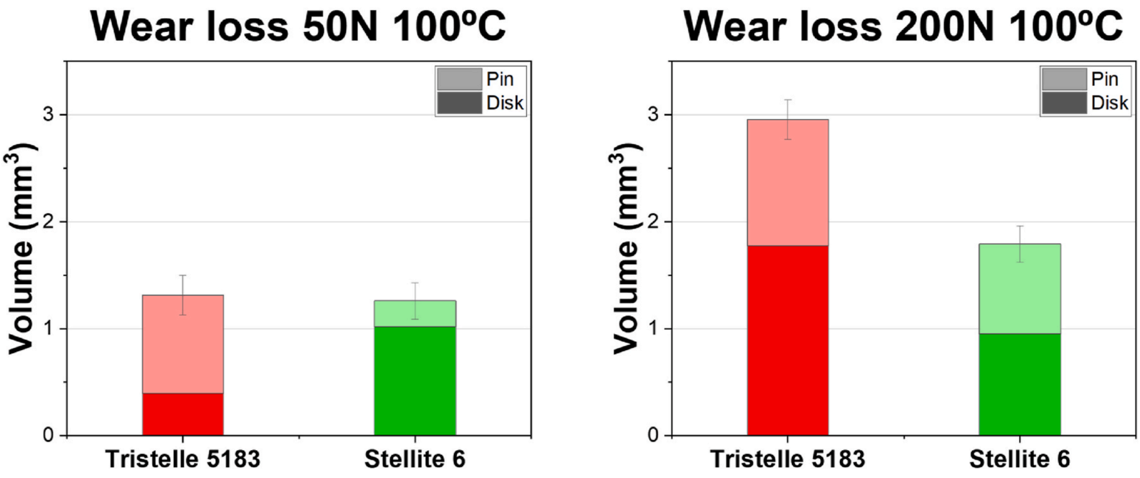

Fig. 10. Wear volume for tests at 100 °C for (a) 50 N and (b) 200 N.

Vickers hardness of the surface of the laser-deposited hardfacings. The HV1 method was used with 15 s loading time for a total of fourteen indents on each sample, taking data points from both directions, parallel and perpendicular to the laser deposition, to obtain the average hardness of the plates.

A FEI Inspect-F50 Field-Emission Gun SEM, with accelerating voltages of 5–20 kV, was used for imaging the starting microstructure and worn surfaces, imaging with both secondary electron (SE) and backscattered electrons (BSE). Chemical analysis was carried out with an Oxford Instruments energy-dispersive x-ray (EDS) detector at 20 kV.

Focused Ion Beam (FIB) was undertaken to obtain site specific cross-sections of the surface, using a FEI Quanta 200 3D dual-beam FIB. The electron-beam mode was operated at 20 kV and 1.2 mA and the ion-beam at 30 kV and 10 pA for scanning mode. The ion-beam current changed during the different steps of the process from 7 nA to 30 pA on the final thinning step. For TEM sample preparation, a FEI Helios Nanolab G3 UC was also used. In this case, the electron-beam mode was operated at 10 kV and the ion-beam at 30 kV and 80 pA for imaging the subsurface. The size of the lamellae produced by this method was 15 × 3 μm with a thickness around 200 nm.

TEM samples were examined on a JEOL JEM F200 transmission electron microscope using a cold field emission gun was used operating at 200 kV. Scanning transmission electron microscopy (STEM) was used to analyse the composition of the samples using the STEM-EDS detector at 200 kV. The JEOL JEM F200 is equipped with a GATAN OneView camera for capturing images, a HAADF detector for dark field imaging during STEM mode and a BF camera for bright field.

3. Results

3.1. Material microstructure

The starting microstructure was investigated in detail using X-ray diffraction, SEM and TEM, given in detail elsewhere [13]. The Tristelle 5183 showed a microstructure comprising austenite dendrites, ferrite, silicide and chromium carbides on the interdendritic spacing and niobium carbides as precipitates (1–50 μm) distributed through the microstructure, Fig. 1a. The Stellite 6 showed a homogeneous dendritic matrix with a eutectic structure of chromium carbides and a cobalt-rich phase in the interdendritic spacing, Fig. 1b. The Vickers hardness of the Stellite 6 was 528 ± 5 kgmm^{-2} while the Tristelle 5183 hardness was 432 ± 8 kgmm^{-2}.

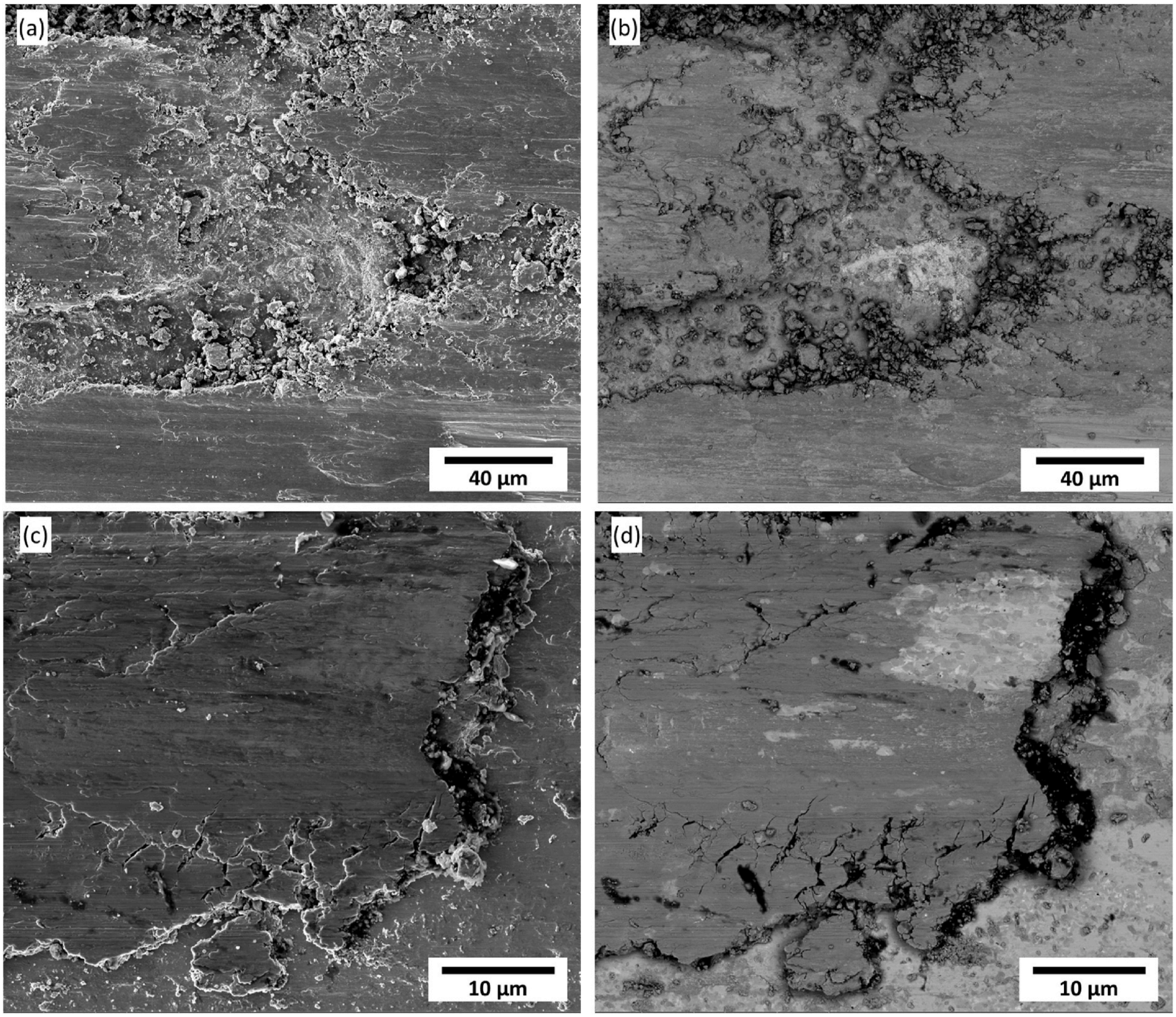

Fig. 11. Secondary electron SEM images (a, c) and backscattered electron images of the same area (b, d) after the tests at 100 °C and 200 N. a,b) Tristelle, c, d) Stellite.

3.2. Friction and wear at room temperature

Repeat tests were undertaken at 50 N for both materials at the start and excellent repeatability was found. Fig. 2a shows the friction behaviour at 50 N. The friction of the Tristelle dropped from ~0.6 at the start of the test to a relatively stable value of ~0.43 throughout the test. In contrast, the Stellite showed a lower initial friction of ~0.35, but this increased rapidly to ~0.85 during the first 2500 s, followed by a gradual rise to ~0.9 at the end of the test. This behaviour was identical on a repeat test.

Fig. 2b gives the friction for the 200 N tests. The CoF for the Tristelle was similar to that observed at 50 N. However, the CoF for the Stellite was substantially lower, starting around 0.35 and gradually rising to ~0.45 at the end of the test. Fig. 2c gives the CoF for the test at 500 N. The Tristelle was again similar to the two lower loads, although there was a gradual rise throughout the test from ~0.32 in the early stages to ~0.35 at the end. In contrast to the lower loads, the Stellite now exhibited the lowest CoF, starting from ~0.32 at the start, staying approximately the same throughout the test.

Fig. 3 gives the wear volume of both pin and disc as a function of load for the room temperature tests. The wear volume was too small to measure at 50 N. At 200 N, Fig. 3a, the Stellite showed the highest combined wear volume. The proportion of wear between pin and disc was different between the two materials, with the Stellite showing the lower disc wear, but much greater pin wear. At 500 N, Fig. 3b, the Tristelle showed a significant increase in wear volume, which was almost double the Stellite. Again, the wear on the Stellite pin was substantially greater than the disc, whereas the wear rates on the pin and disc were relatively similar for the Tristelle.

Fig. 4 gives SEM images of the worn surface after the 50 N test. A wear scar was seen, although the wear volume was too small to measure. Longitudinal grooves were observed in the sliding direction of the Tristelle, Fig. 4a, with accumulate wear debris on the surface that were of similar size to the grooves, suggesting the grooves were formed by these particles being pushed through the surface. The Stellite surface was much smoother than the Tristelle, Fig. 4b, but was covered in what appeared to be an oxide layer which showed evidence of stick slip behaviour and was regularly found becoming detached from the surface. Such stick slip will have contributed to noise in the friction signal.

The characteristics and morphology of the wear scars of the Tristelle at 200 N was similar to the 50 N tests but the wear scar was deeper, and the wear rate was now measurable. There was extensive grooving, but also surface layers appeared to have built up that formed the contacting surface, with accumulation of large amounts of wear debris, Fig. 5a. There was a significant amount of oxidised wear debris at the edge of the wear scar. The Stellite wear scar was significantly different at 200 N compared to 50 N. At 200 N it exhibited extensive plastic grooving, but the stick-slip oxide layer was not present, Fig. 5b. Small wear particles

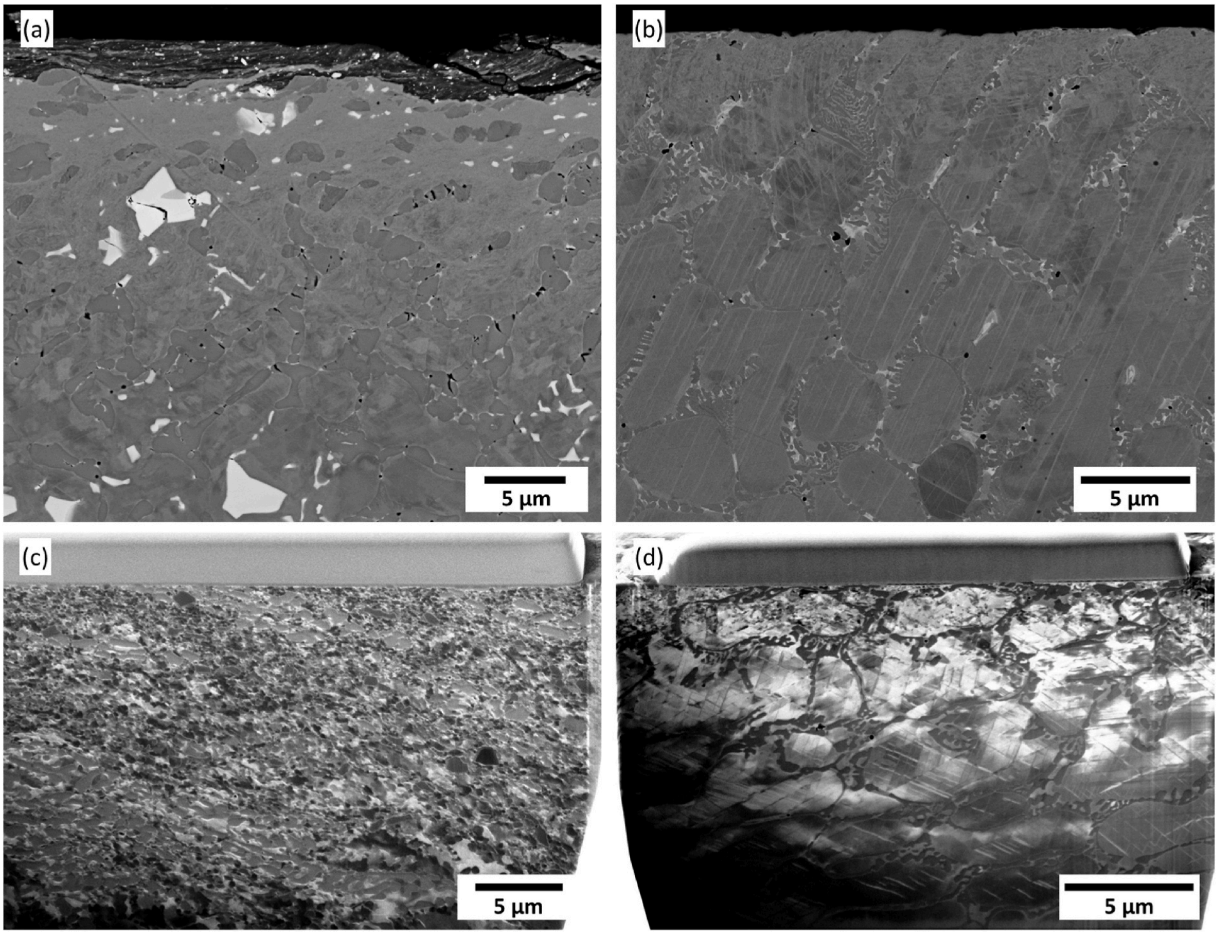

Fig. 12. Backscattered electron images of cross-sections of the (a) Tristelle (b) Stellite pins after the 50 N sliding wear tests at 100 °C. FIB sections of the disc with ion channelling contrast, (c) Tristelle 5183 (d) Stellite 6.

and mechanically mixed layers were evident on the worn surface.

The same features were seen at 500 N as 200 N, but more extensive grooving was seen, Fig. 6, which was especially visible on the iron-based alloys where there was a considerable amount of plastically deformed material on the edges of the wear scar. Mechanically mixed layers compressed on the surface were extensively observed for both alloys as well as fragmented wear debris.

Cross-sections of the worn surface were undertaken using FIB. Fig. 7 gives ion channelling contrast images of the room temperature tests at 50 N. The section from the Tristelle, Fig. 7a was removed from a region that showed a surface pad of agglomerated wear debris such as that in Fig. 4a. A thick (~5 μm) mechanically mixed layer is shown on the surface, with a very fine structure and containing fragmented carbides. Below this, there is a layer that has clearly undergone significant microstructural refinement. In contast, the Stellite surface, Fig. 7b, showed minimal microstructural change, except some evidence of planar features that were either twins or martensite plates or both.

A cross-section of the tests at 500 N is given in Fig. 8. The surface of the Tristelle was comparatively flat but extensive plastic deformation and refinement of the dendritic microstructure down to 10 μm from the surface had occurred, Fig. 8a, with evidence of surface damage down to 15 μm. The larger niobium carbides closer to the surface were extensively cracked, which led to complete fragmentation of the carbides closest to the surface. Interestingly, the metal matrix had flowed around these particles such that the carbide/matrix interface remained intact. The surface of the Stellite at 500 N looked quite different to the Tristelle, Fig. 8b. The degree of deformation was considerably less in the Stellite. There was some evidence of cracking of the hard second phase particles, but this was limited. Regions of surface delamination were observed, associated with loss of the matrix.

3.3. Friction and wear at 100 °C

The coefficient of friction for tests at 50 N and 100 °C are shown in Fig. 9a. The CoF for the Tristelle was around 0.38 for the duration of the tests, dipping slightly towards the end. The Stellite showed a small rise in CoF at the start of the test from ~0.28 to ~0.35, followed by a steady fall during the test to around 0.25 at the end. This is very different to the values ~0.9 seen for the room temperature tests with the same load of 50 N. Fig. 9b gives the CoF for the 200 N tests at 100 °C. The initial friction for the Tristelle was high at 0.5, but this fell quickly to ~0.36 and remained at that value until the end of the test. The Stellite started just below 0.3 followed by a gradual rise to ~0.4 at the end of the test.

The combined and individual pin and disc volume losses for the reciprocating sliding wear tests at 100 °C for 50 N and 200 N are shown in Fig. 10. At 50 N, the Tristelle exhibited greater loss of material than the Stellite when the pin and disc wear volumes are combined. At 200 N tests, the iron-based alloy exhibited almost double the material removal compared to the Stellite.

SEM micrographs showing the worn surface morphology after testing at 200 N 100 °C are given in Fig. 11. The features observed at this load were similar to those found at 50 N. The surface was dominated by plastically deformed grooves, with plastic deformation evident at the edge of the wear scars. The extent of this was greater for the Tristelle compared to the Stellite. A marked difference between the 100 °C tests and the room temperature tests was the extensive presence of surface

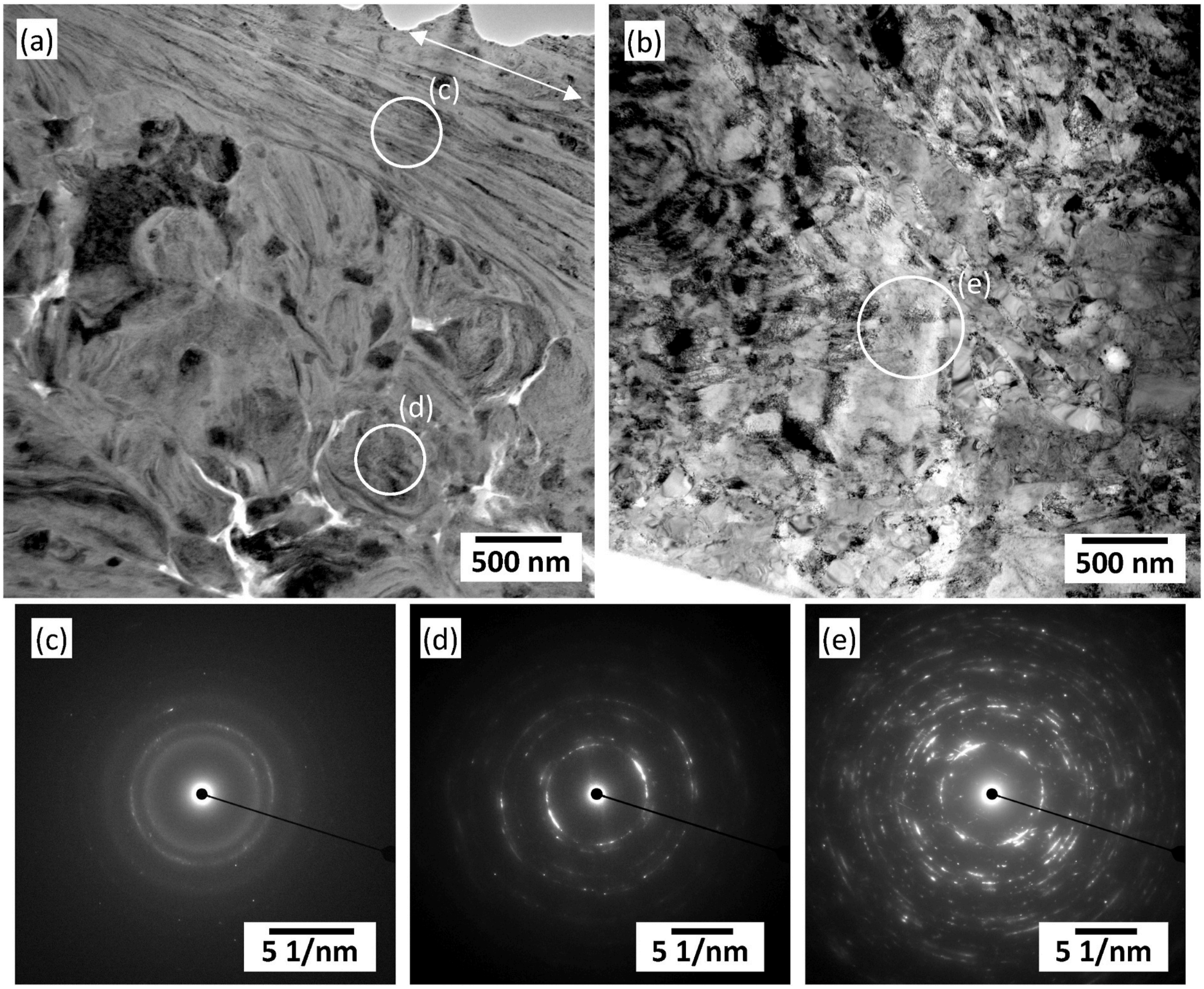

Fig. 13. TEM bright field images from a FIB surface cross section of the Tristelle disc at 50 N sliding wear tests at 100 °C. (a) oxide layer. (b) heavily deformed nanocrystalline layer. Diffraction patterns taken from the regions indicated.

layers which appear to be mechanically mixed material of metal and oxide, Fig. 11 b,d, which appears to form the contacting surface. Regions where this layer became detached were evident for the Tristelle Fig. 11 a,b, but less obvious for the Stellite.

Fig. 12 gives SEM images of cross sections of the worn surface tested at 50 N at 100 °C. The Tristelle shows a ~ 3 μm surface layer of mechanically mixed material formed from oxides, metal and small fragmented niobium carbides (characteristic white contrast). This layer is mostly adhered to the substrate material where a 15 μm plastically deformed layer can be observed below. Below this there is a region that has clearly been plastically deformed, but which shows minimum contrast. Below this cracking can be seen in both the niobium carbides and the brittle silicide phase (mid grey contrast). A similar region showing the deformed region showing minimal contrast in Fig. 12a was examined using ion channelling contrast in Fig. 12c. This shows the extensive plastic deformation that occurred that has broken up the eutectic structure and resulted in significant refinement of the structure.

The Stellite 6 again showed quite different features to the Tristelle, Fig. 12 b,d. The surface was quite flat, and the extent of plastic deformation was relatively small. There is slightly deformed layer, about a 5 μm thick, with small areas of delaminated material on the surface. Linear features within the grains have arisen from planar slip bands or twins which extend to a depth of 20 μm. These are somewhat clearer in the ion channelling image in Fig. 12d.

TEM sections were removed by FIB from the surface of both materials tested at 50 N at 100 °C, Fig. 13. An overview DF-STEM image of the outermost region is shown in Fig. 13a, showing the presence of a thick mechanically mixed layer of different phases. The extreme outmost layer showed extensive plastic deformation parallel to the sliding direction with a very fine structure, which electron diffraction indicated is semi-amorphous (Fig. 13c). Below this is a similar region, but where the flow of material was much more random, with coarser particles and extensive voiding. This region had increased crystallinity as shown by the diffraction pattern in Fig. 13d. The area immediately below the mechanically mixed layer is shown in Fig. 13b, which shows a fine nanocrystalline layer. Some secondary phases which appear to be the M_7C_3 eutectic-type carbides were observed. The diffraction pattern from this region Fig. 13e shows the degree of crystallinity with minimal crystallographic texture in this area.

Further analysis of the mechanically mixed layer, shown in Fig. 13a, was carried out using high spatial resolution EDS, Fig. 14. This confirmed that the layer was predominantly an oxide. It shows how the niobium carbides, which were originally 5–30 μm in size, had become extensively broken up into particles typically 10–100 nm in size that were uniformly dispersed throughout this layer. In addition, fragments of the M_7C_3 particles can be seen through the Cr map, with a similar size to the NbC fragments.

Fig. 15 gives a similar section from the Stellite sample. This showed a dramatic difference to the Tristelle in that minimal microstructural change was observed. The microstructure below the contacting surface still showed the dendritic matrix and eutectic carbides with minimal plastic deformation. The main mechanism observed to be

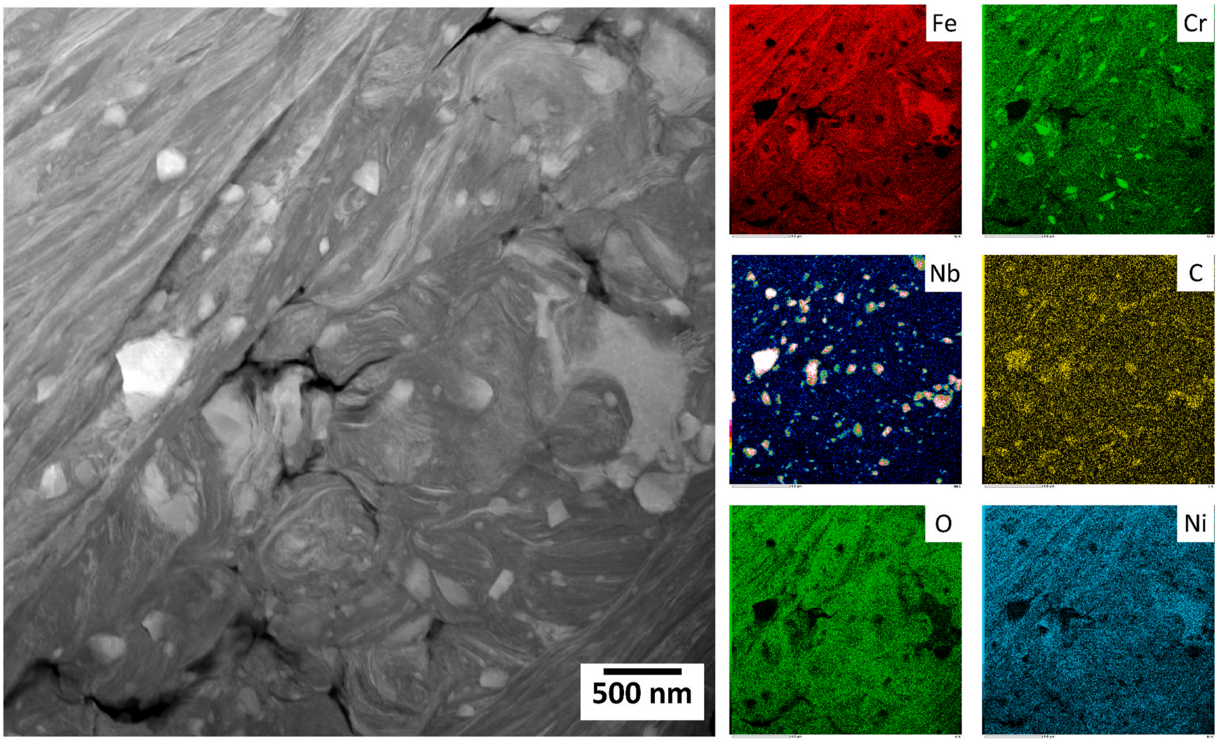

Fig. 14. STEM-EDX maps of the main elements forming the mechanically mixed surface layer on the Tristelle disc from a cross-section after the 50 N tests at 100 °C.

accommodating the strains seems to be the strain induced transformation of α-Co into ε-Co, as shown by the electron diffraction pattern, with the ε-Co appearing as the long, thin needle like features in Fig. 15a. An example of a eutectic carbide is shown in Fig. 15c with corresponding diffraction pattern in (d), indexed as Cr_7C_3, which had not undergone any microstructural change with wear.

3.4. *Friction and wear at 200 °C*

Fig. 16 gives the friction coefficient for the 50 N and 200 N tests at 200 °C. At 50 N, the friction was relatively stable for both materials, with the Tristelle at ~0.48 and the Stellite at~0.4, both slightly higher than the tests at 100 °C. At 200 N, the friction for the Tristelle was similar to that at 50 N, but the Stellite fell to a stable value of ~0.31 throughout the test.

The combined wear volume for 50 N at 200 °C was ~1 mm^3 for both materials, Fig. 17a, which is lower than experienced at 50 N, 100 °C. At 200 N, the combined wear volume was significantly higher than at 50 N, Fig. 17b, with the Stellite exhibiting slightly more wear than the Tristelle.

Fig. 18 shows backscattered electron images of the worn surfaces at 200 N, 200 °C, with the two materials similar to each other and similar to the surfaces at 50 N. Extensive grooving was present. Oxide (darker contrast) was extensively mixed in the surface and loose oxide wear debris was also present. The oxide regions on the Tristelle were extensively cracked, but less so on the Stellite.

Fig. 19 gives cross-sections of the worn surfaces at 200 N, 200 °C. As with other test conditions, the NbC in the Tristelle was extensively cracked at the surface. Surface oxide layers were present, deformed along with the metal forming a composite structure. Surface delamination was also evident. Below this, the metal had been extensively deformed, obscuring the original as-cast structure. The Stellite also showed an oxide/deformed metal composite structure, but this was not bonded to the surface, Fig. 19b. There was some evidence of surface deformation, extending to a depth of ~15 μm, but this was much less than for the Tristelle.

3.5. *Friction and wear at 300 °C*

Fig. 20 shows the friction behaviour for loads of 50 and 200 N. In both cases, the CoF for the Stellite was much lower than for the Tristelle, being stable at around 0.3 throughout. At 50 N, the CoF of the Tristelle was stable around 0.5, but at 200 N, it rose from an initial value of ~0.44–~0.7 at the end of the test.

Fig. 21 gives the wear volumes at 300 °C. For a load of 50 N, the wear volumes were similar for the two materials, and similar in value to that observed at 100 °C. A significant rise in wear volume was observed at 200 N, with the Tristelle exhibiting significantly more wear than the Stellite, Fig. 21b.

Fig. 22 gives SEM images of the worn surface of the samples for the 200 N test at 300 °C. The Tristelle surface was similar to that at lower temperatures, namely extensive grooving, oxides mixed into the surface and wear debris being formed at the edge of the grooves. In contrast, the Stellite surface was quite different, exhibiting a comparatively smooth surface, which was predominantly metallic, with fine angular oxide particulate distributed on the surface, which had not been deformed into the surface, Fig. 22b.

Fig. 23a and b, gives cross-sections of the pins for the 200 N test at 300 °C. The Tristelle, Fig. 23a, looked similar to surfaces at lower temperatures, namely fractured NbC, deformed surface layers comprising a mixture of oxide, metal and fine fragmented NbC. The total depth of damage was ~45 μm. The Stellite showed a surface layer of a composite of deformed metal and oxide, Fig. 23b, similar to that seen under lower temperatures. Below this there was a deformed layer extending to approximately 15 μm below the surface, below which some low strain features such as twins and martensite plates were observed. Fig. 23c and d gives ion channelling contrast images from cross-sections of the disc for the 200 N test at 300 °C. The features on the Tristelle surface are similar to those on the pin, namely an oxide/metal composite layer, a heavily deformed layer and fractured NbC. The Stellite showed much less damage, Fig. 23d, with microstructural refinement leading to a rudimentary nanocrystalline layer in the outer ~5 μm. No oxide was seen on the surface. Below this, there was little evidence of deformation.

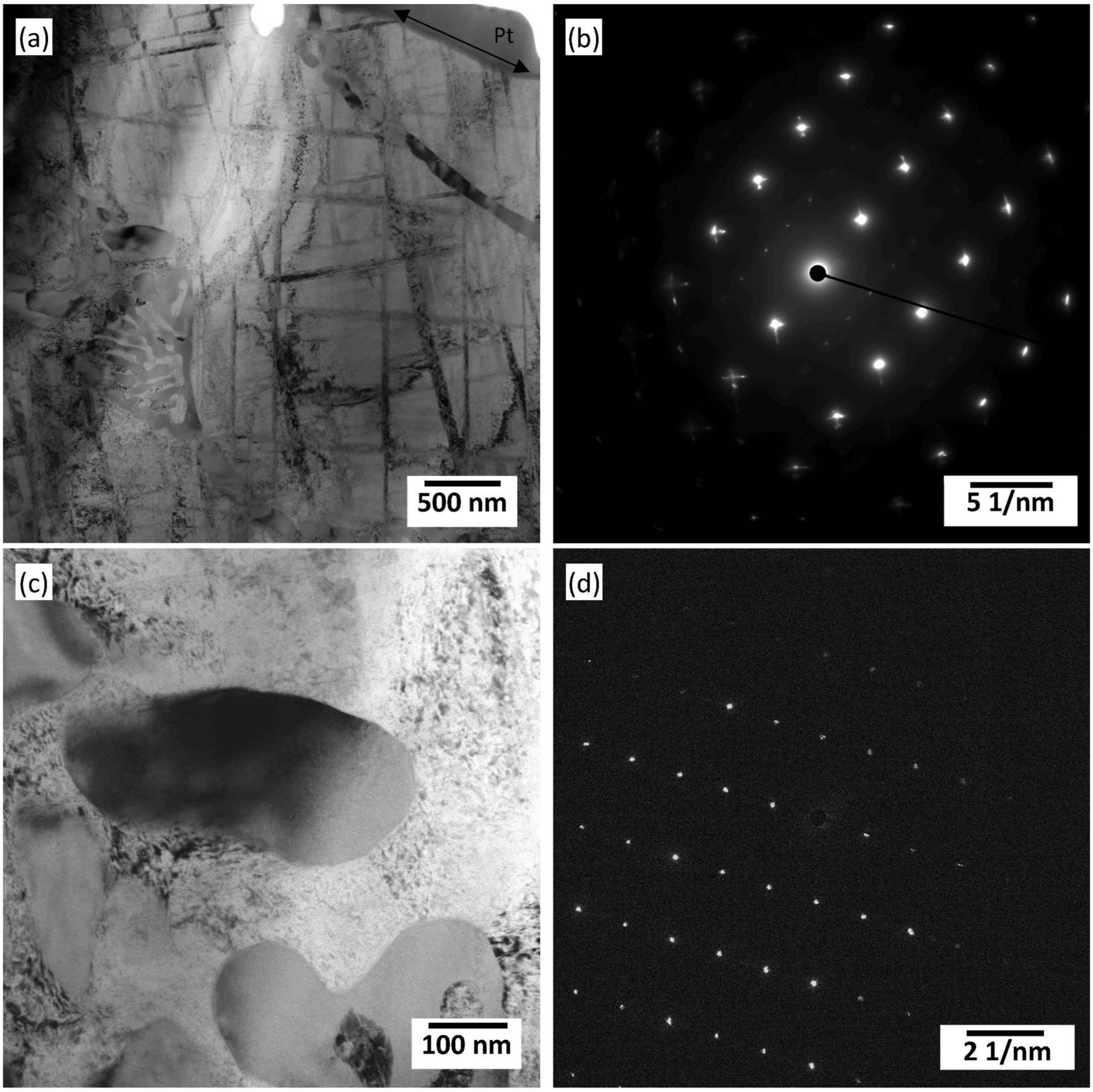

Fig. 15. BF-TEM (a,c) micrographs and SADP (b,d) from a sample taken parallel to the sliding direction of the Stellite disc after the 50 N test at 100 °C.

Fig. 24 gives a bright field TEM image from the Tristelle disc after testing at 200 N at 300 °C. Fig. 24a shows a very fine nanostructure which comprises metallic regions, indexed as γ-Fe, with oxide also present and numerous fragmented NbC particles. Fig. 24b shows a STEM image from an adjacent region showing the complexity of the surface structure with two types of mechanically mixed layers being present. The associated elemental maps show that the right-hand layer is rich in oxygen, while the left-hand layer contains much less oxygen. The Cr map shows the distribution of the fragmented M_7C_3, while the Nb map shows the distribution of the fragmented NbC.

Fig. 25 gives similar TEM images for the Stellite under the same conditions as Fig. 24. Fig. 25a shows the development of a classical nanocrystalline layer adjacent to the surface, while Fig. 25 b shows planar defects that are associated with the creation of a strain-induced transformation of the γ-Co phase into the hexagonal ε-Co.

4. Discussion

4.1. Friction behaviour

The friction coefficient of the Stellite tested at 50 N at room temperature was particularly high, rising rapidly from an initial value of 0.3 up to 0.85 and then steadily increasing reaching 0.9 at the end of the test, Fig. 2a. This was substantially higher than the Tristelle, which had a friction of ~0.35 throughout the test under the same conditions. However, when the Stellite was tested at 200 N at room temperature, the friction was much lower, starting at 0.35, increasing to ~0.4 at the end of the test. This has also been observed in previous studies by Zhu et al. [14], where a Stellite 6 layer was deposited using plasma transferred arc welding (PTAW) and subjected to a ball-on-disk test using loads of 5–15 N at room temperature. They found that the CoF was high under these conditions and dropped when the temperature was increased to 300 °C. Thus, the high friction in the 50 N test, which was repeatedly found, needs explaining. Both materials tested at 50 N showed an oxide on the worn surface and the nature of that oxide would determine the adhesion between the surfaces and therefore strongly influence the friction. The oxide layer on the Stellite at 50 N was different in nature to the ones observed under higher load or higher temperature. The oxide, with thickness of around 0.8 μm, had a layered morphology characteristic of stick-slip, Fig. 4b, which suggests that the high friction was a result of strong adhesive forces between the two surfaces. In contrast, the Tristelle exhibited a thick, well adhered oxide layer, Fig. 7, that appeared to form the contacting asperities, Fig. 4a. Clearly, this oxide had an inherently lower friction than that formed on the Stellite at 50 N.

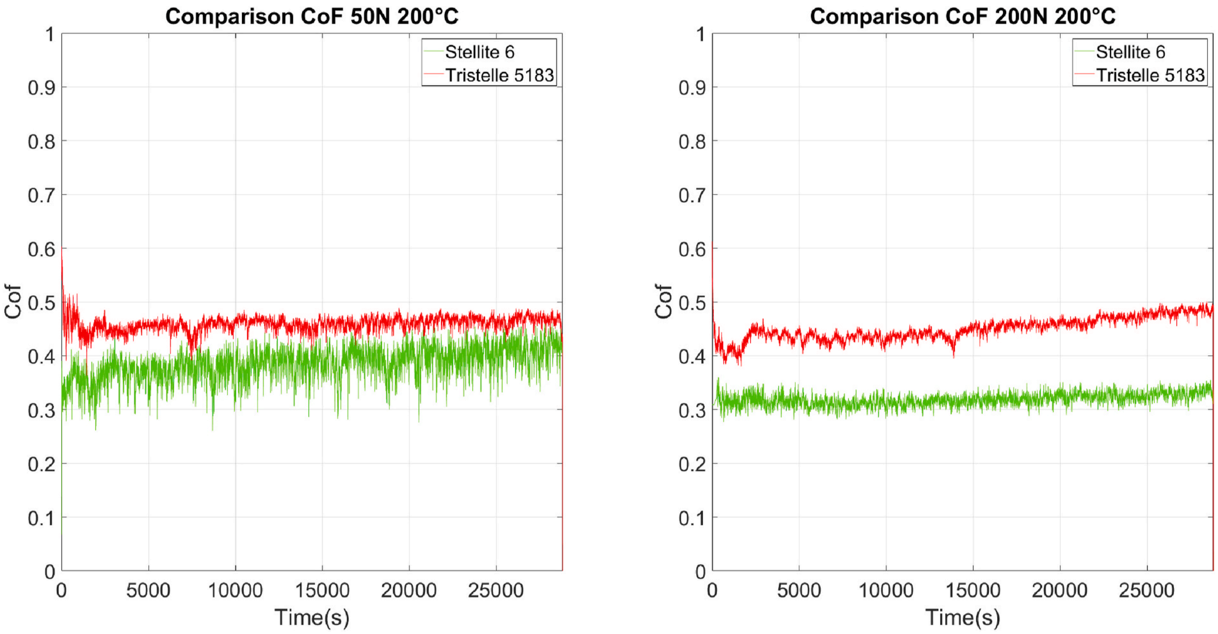

Fig. 16. Coefficient of friction for the tests at 200 °C for (a) 50 N and (b) 200 N.

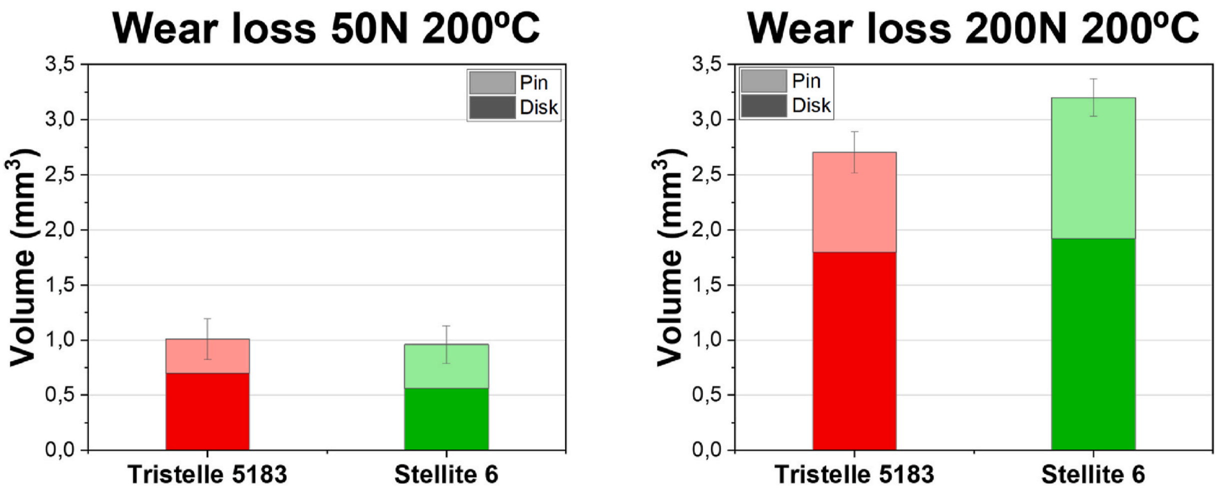

Fig. 17. Wear volumes at 200 °C for (a) 50 N and (b) 200 N.

The friction coefficient of the Stellite 6 alloy was in the range 0.3–0.4 for the remainder of the test conditions, which is remarkably stable and low given the severe test conditions. Indeed, the lowest friction was observed at 200 and 300 °C for a load of 200 N, where the friction was ~0.3. Persson et al. [15] investigated the self-mated high load dry sliding of Stellite 21 at room temperature and found a stable low friction of 0.2, which is slightly lower than the values observed in the current work. The low friction was attributed to the formation of thin Co-enriched tribofilm, where the basal planes of the hcp structure were strongly aligned parallel to the surface, giving easy shear of the surface. In related work, Persson et al. [16] found that for Stellite 21 the friction was lower and more stable at 250 °C compared to room temperature, which is very much in-line with the observations reported here. However, they were not able to explain this observation.

The friction will be influenced by the adhesion between the two surfaces, which is dominated by the mechanically mixed oxide layers, and by deformation of the surface, both in the mechanically mixed layer and also in the substrate. It is difficult to know what the adhesive component of friction is, but clearly for the Stellite at elevated temperature and high load, it was quite small. The oxide on the surface of the Stellite was rarely integrated into the surface, rather it tended to be detached, e.g. Fig. 13b, although in some cases it had become fully integrated with the deformed surface, Fig. 23b. In many cases, the surface was free from oxide, Figs. 7 and 12 b,d and 23d. The lowest friction recorded was at 200 N at 300 °C, where the oxide was only present as isolated particles on the surface, suggesting the oxide did not strongly contribute to the friction.

In addition to the adhesive component of friction, it is also important to consider the deformation component. As noted above, where the fcc α-Co starting structure is transformed to a hcp ε-Co, and a strong texture is formed with the basal planes parallel to the sliding direction, then a low friction coefficient is found [15]. In the current work, the worn surface of the low load tests barely showed any deformation, and the structure remained fcc α-Co, e.g. Fig. 7d and 12d. The fcc structure is associated with higher friction, as shown in Fig. 2a. However, at the higher loads then extensive transformation from fcc α-Co to hcp ε-Co was observed. This was associated with a strong basal texture as shown in Fig. 25a for the 200 N test at 300 °C. The easy shear along the basal

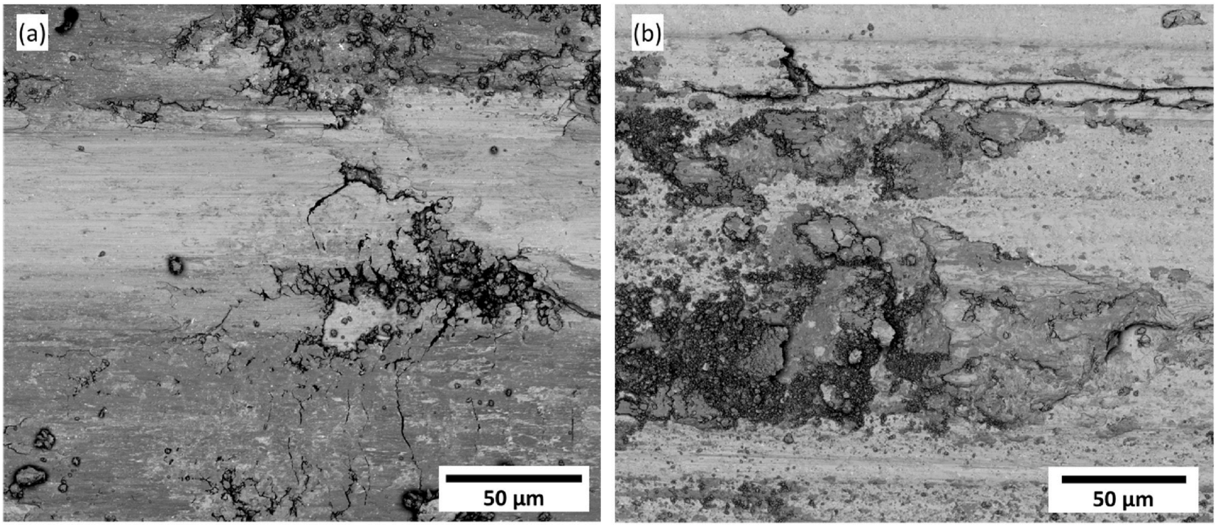

Fig. 18. Backscattered electron images after the tests at 200 °C and 200 N. a) Tristelle, b) Stellite.

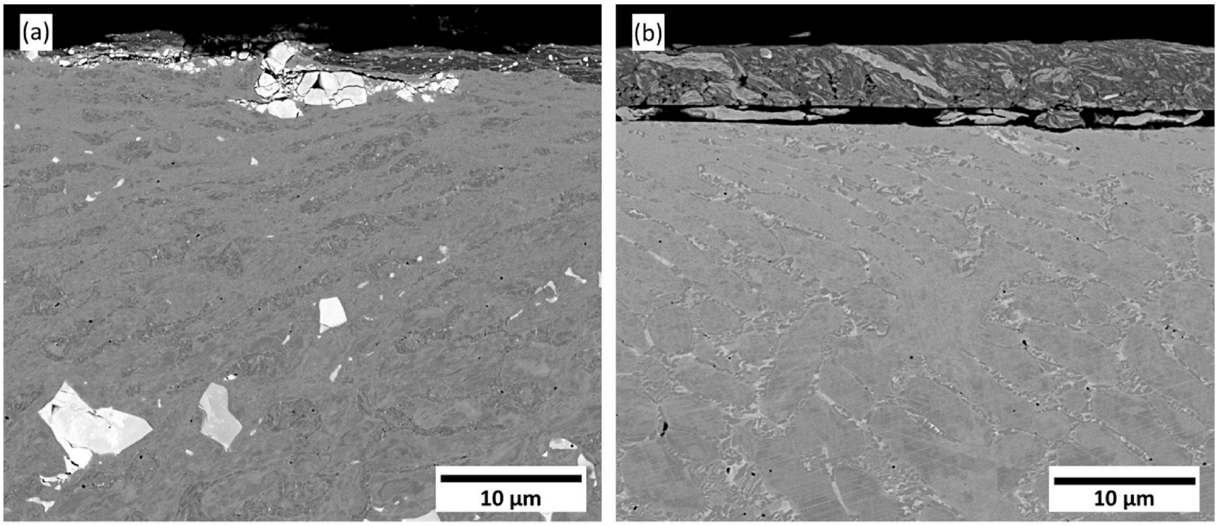

Fig. 19. Backscattered electron images of cross-sections of (a) Tristelle 5183 (b) Stellite 6 pins after the 200 N sliding wear tests at 200 °C.

planes will have contributed to the low friction values seen for these conditions.

The friction of the Tristelle was always higher and less stable than the Stellite, except the room temperature test 50 N. The oxide on the surface of the Tristelle was generally integrated into the surface forming a complex mechanically mixed layer of oxide and heavily deformed metal, Fig. 12 c,d, 13a, 23a. In addition, this mechanically mixed layer contained extensive fractured carbides, both of NbC and M_7C_3, Figs. 14 and 25. It is this complex structure that dictated a higher friction in the Tristelle compared to the Stellite, with an unstable value of 0.7 recorded for the test at 300 °C with a load of 200 N.

4.2. Wear behaviour

The specific wear rates for both materials are given in Fig. 26. The wear behaviour at 50 N as a function of temperature was similar for both materials. Wear volumes increased from being immeasurable at room temperature to ~1.5 mm^3 at 300 °C. The specific wear rate did not change appreciably between 100 and 300 °C, being similar for both materials, although both showed a drop for 200 °C compared to the other temperatures. Although both materials exhibited similar wear rates, the worn surface morphology was very different and the microstructure below the worn surface was very different.

The Tristelle exhibit a surface oxide under all test conditions. This tribolayer appeared to comprise fine wear debris particles that agglomerate, are plastically deformed, and adhere to the worn surface and appear to form the contacting asperities. Cross-sections through the oxide showed how complex its structure is. At 50 N and room temperature, the oxide contained numerous fragmented NbC and M_7C_3 particles, showing the mechanically mixed nature of its formation Fig. 7a. It was well adhered to the substrate metal, and although it contained numerous cracks, it exhibited a high packing density. This oxide formation followed the classic behaviour as described extensively in Refs. [17–20].

The behaviour of the Tristelle was similar at 100–300 °C for the 50 N load. At 100 °C the oxide layer also contained metal slivers showing how both oxide and metal had been deformed together, Fig. 12. The complex nature of this deformation is shown clearly in Fig. 13, where the intimate nature of the oxide and metal deformation can be seen. In the outer region the oxide was aligned parallel to the surface, but lower down the swirling nature of the deformation can be seen, which, along with the cracking, shows how this layer was formed by the agglomeration of fine

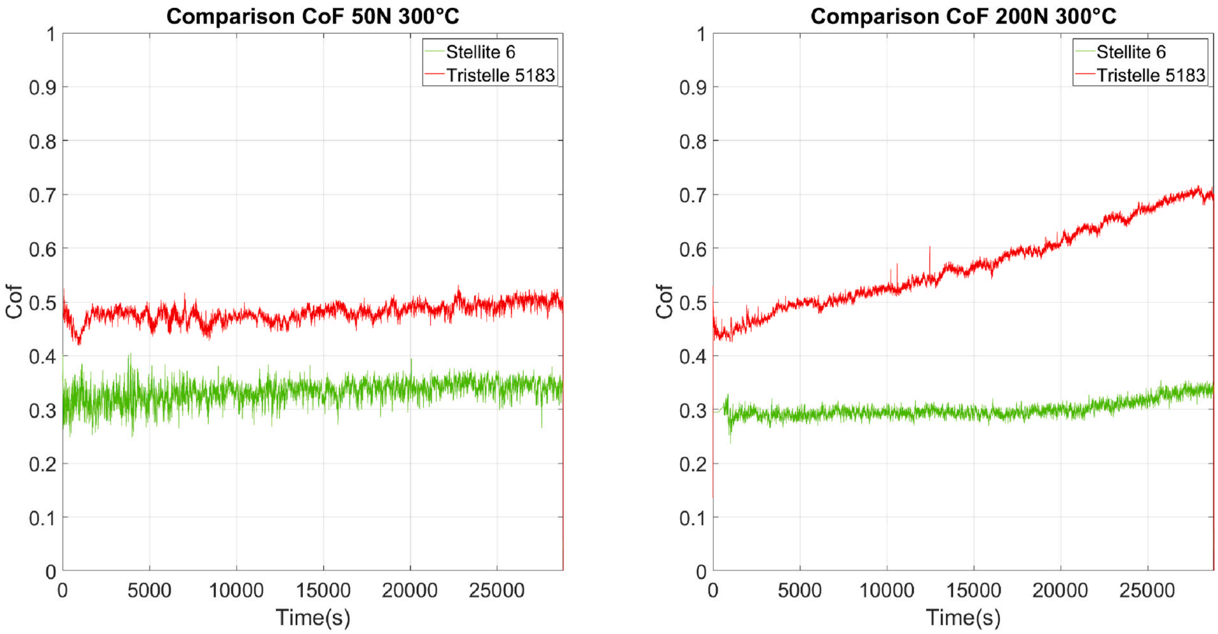

Fig. 20. Coefficient of friction for the two materials for 50 and 200 N tests at 300 °C.

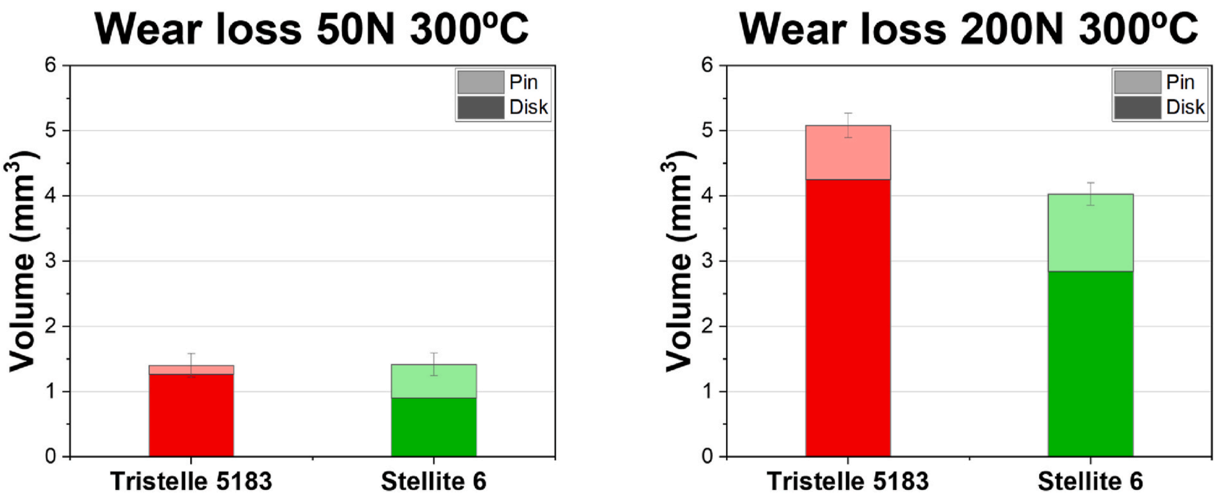

Fig. 21. Wear volume of the Tristelle and Stellite alloys after 50 N and 200 N tests at 300 °C.

wear debris particles. Interestingly, although the tribolayer clearly contained extensive oxygen, Fig. 14, the diffraction patterns still indexed as γ-Fe. The manner in which the NbC had been fractured well below the worn surface but had become greatly refined in size from around 1-50 μm at the start to a nm size range in the tribolayer shows how the matrix was able to flow round the fractured particles and maintain cohesion between matrix and carbide. Thus, the potentially highly detrimental nature of the NbC fracture had been mitigated to some extent. However, wear debris was clearly generated from this tribofilm and cracking was often associated with NbC particles e.g. in Fig. 12a.

The oxide on the Stellite was quite different to the Tristelle at 50 N and indeed the other loads. The oxide on the worn surface of the test at 50 N at room temperature exhibited stick slip behaviour, promoting high friction, as discussed before. Large regions were free of an oxide tribofilm, e.g., Fig. 12 c, d. At higher test temperature, regions of tribofilm integrated into the worn surface were found, but this was far less than observed for the Tristelle. This behaviour was somewhat similar to that observed by Carrington et al. [11], who tested a HIPed Stellite 6 at room temperature and 250 °C, but who used lithiated, deoxygenated, deionised water in which the oxygen content was very low.

The extent of surface deformation was far greater for the Tristelle compared to the Stellite, but this did not change appreciably with temperature for the 50 N tests for either material. The Stellite showed minimal deformation, with planar features present, Fig. 7b, that were mostly ε-Co martensite plates, Fig. 15, which has been observed in previous studies [2,9,11,21]. The presence of the M_7C_3, which remained undeformed in the samples studied, is also believed to aid the accommodation of plastic deformation by generating multiaxial stress states within the matrix, thus promoting deformation systems that will contribute to work hardening. The Tristelle did show some plastic deformation, that extended someway below the worn surface, e.g. ~10 μm for the 50 N test at 100 °C. This resulted in the break-up of the original as-cast microstructure, forming a rudimentary nanocrystalline structure, Fig. 12b, which can be contrasted with the minimal deformation for the Stellite in Fig. 12d. Moreover, the deformation resulted in fracture of the NbC to a long way below the worn surface, but it was interesting the manner in which the matrix flowed around the carbide,

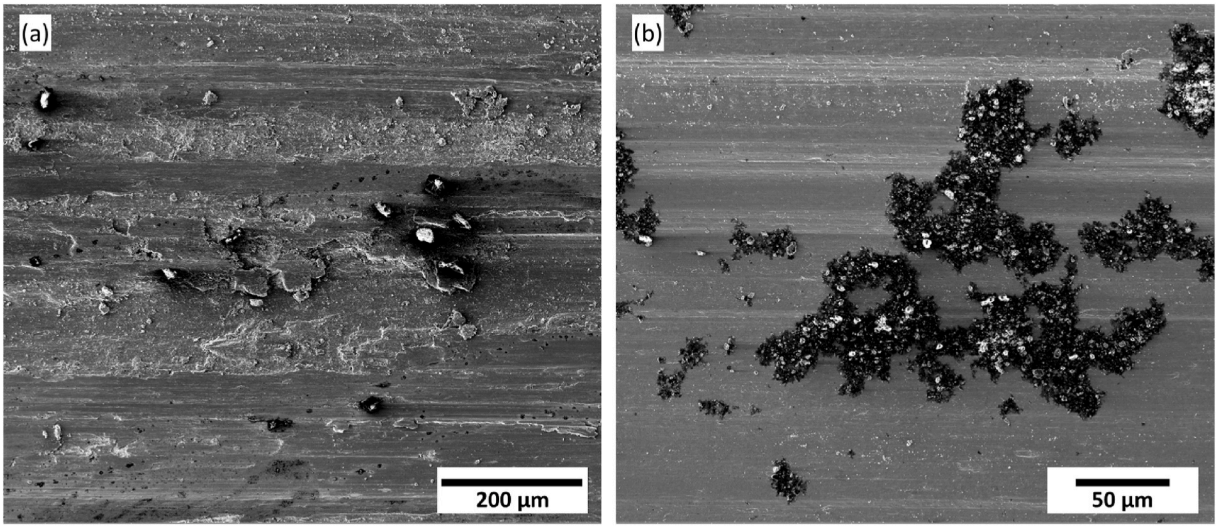

Fig. 22. Secondary electron SEM images after the tests at 300 °C and 200 N. a) Tristelle, b) Stellite.

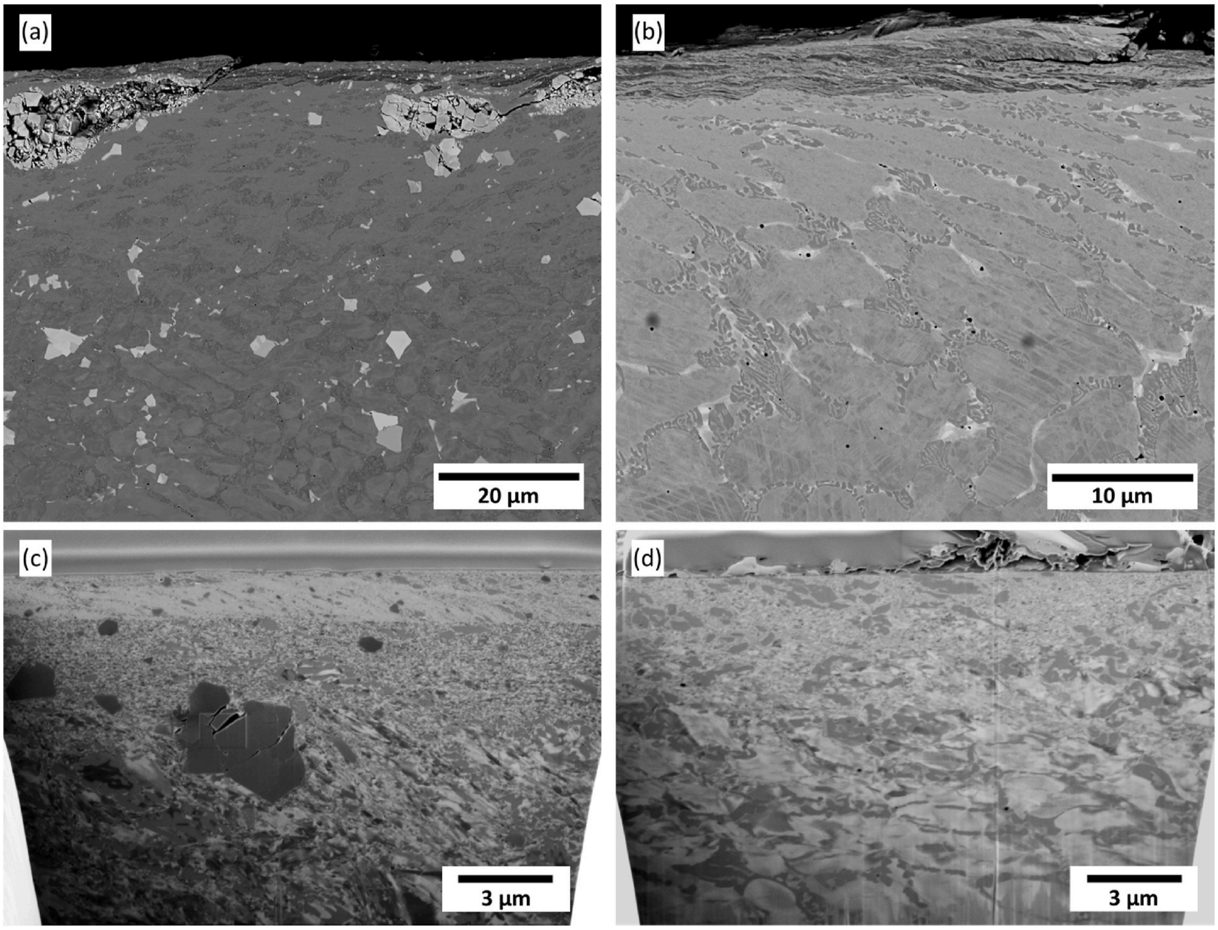

Fig. 23. Backscattered electron images of cross sections of (a) Tristelle 5183 (b) Stellite 6 pins after the 200 N sliding wear tests at 300 °C. Ion channelling images from FIB sections from the disc c) Tristelle, d) Stellite.

maintaining cohesion between the two. The silicide was also fractured to a similar depth to the NbC, but this did not lead to the same scale of fragmentation, Fig. 12a.

The wear rates at the higher load of 200 N were strongly temperature dependent for both materials, Fig. 26. The Stellite exhibited just over a doubling in wear volume between room temperature and 300 °C, whereas the Tristelle showed a 3x increase in wear rate. The increase in specific wear rate with temperature for both materials indicates that the wear process was becoming more severe. There is little data on the temperature dependence of wear for the Tristelle, but Carrington [9] only observed an increase in wear by a factor between 1.1 and 2.1x with an increase in test temperature from 20 °C to 250 °C. In contrast, there

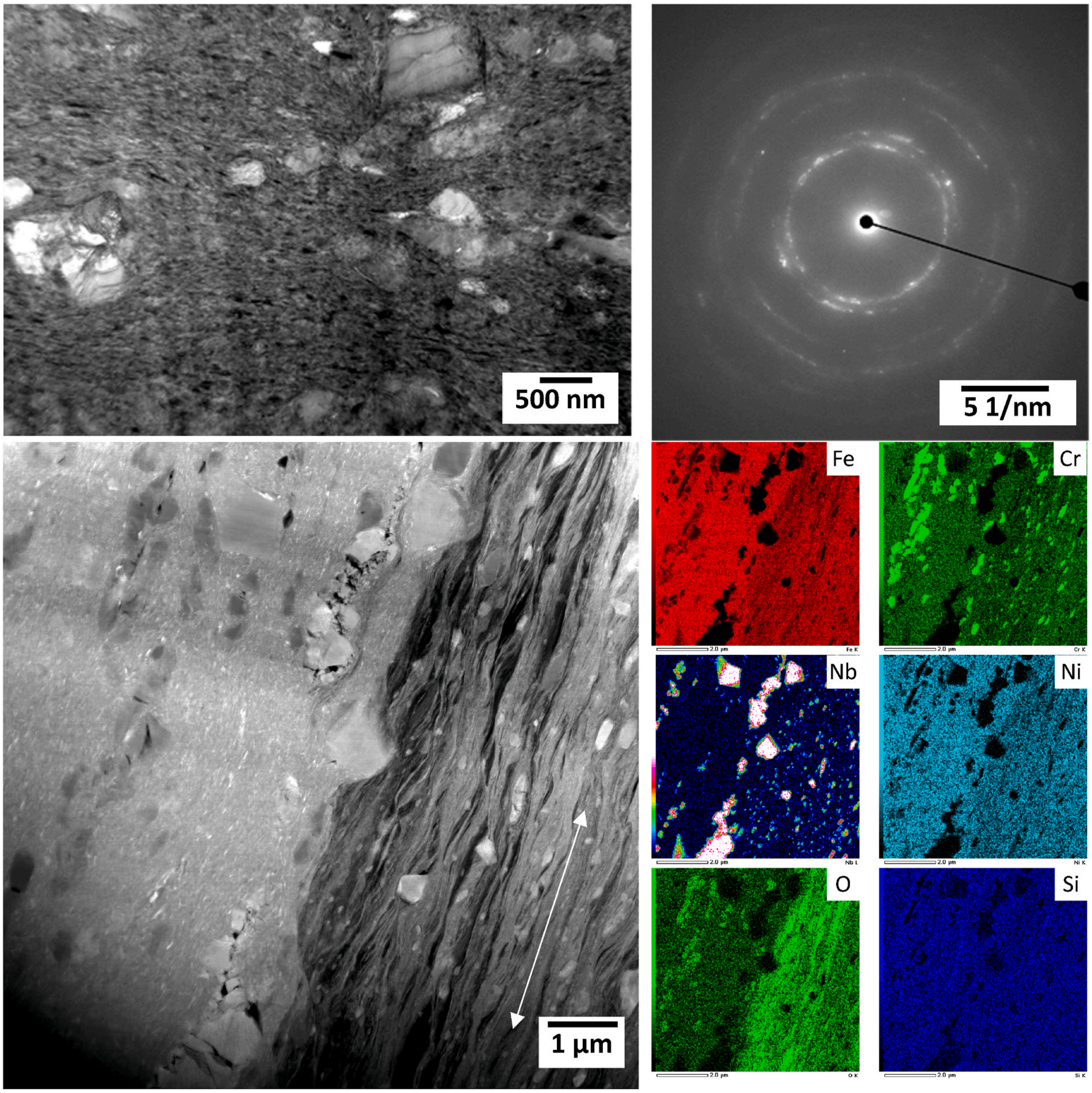

Fig. 24. a) Bright field TEM image and corresponding diffraction pattern from the Tristelle disc after the 200 N tests at 300 °C. b) STEM bright field image and corresponding EDX maps of the outer mechanically mixed layer.

have been several studies on Stellite which have shown a strong temperature dependence of wear rate. For example, Carrington et al. observed an increase of between 16.5x and 38.7x in going from 20 °C to 250 °C, which is much greater than observed here, although their Hertzian contact stresses were higher and they were investigating lubricated sliding rather than the dry sliding used here. Nevertheless, the wear rate of the Stellite was around half that of the Tristelle [9].

The higher load induced an oxide based tribolayer on the surface of the Stellite that showed similarities with the Tristelle, namely it appeared to comprise fine wear debris particles that agglomerated, were plastically deformed and appeared to form the contacting asperities, Fig. 11c and d. However, cross-sections through the surface showed that this tribolayer was often not attached to the substrate, for example, Fig. 13 for the 200 N test at 200 °C. However, there were examples where the tribolayer had deformed with the metal surface and contained metal slivers showing how both oxide and metal had been deformed together and was fully integrated into the surface. This behaviour was similar in some ways to that of Crook and Li [22] who observed the formation of a protective oxide glaze layer at temperatures greater than 250 °C. Stott et al. [23] also reported that at temperatures above 250 °C, gave a stable thermally softened oxide glaze layer formed which acted to retard the rate of wear. However, in the current tests no glaze layer was formed at any temperature.

The oxide surface on the Tristelle did not fundamentally change with an increase in temperature, remaining as a layer that was largely adherent to the substrate, either as a discrete tribolayer (e.g. Fig. 23c) or as a mechanically mixed layer, inter-twined with the matrix (Fig. 23a). Several examples of where this layer was delaminating could be found, which was sometimes associated with break-up of large NbC particles (Fig. 13a). The structure of the tribolayer in Fig. 24a is similar to that reported by Carrington [9] for the sliding of HIPed Tristelle alloy lubricated by lithiated deoxygenated water.

At 200 N the extent of deformation was substantially higher than at 50 N for both materials and increased with temperature, but with much greater deformation seen for the Tristelle compared to the Stellite. The microstructural changes below the worn surface could be divided into

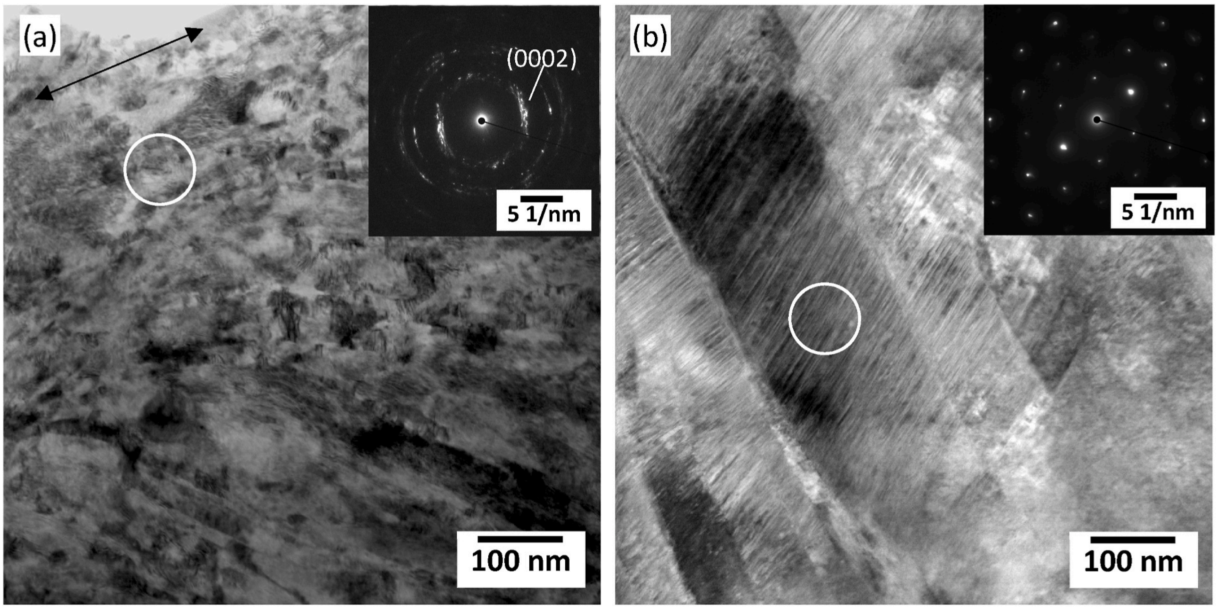

Fig. 25. a) Bright field TEM images and insert corresponding diffraction pattern from the Stellite after the 200 N tests at 300 °C, showing a fine nanocrystalline structure (a) and fine scale twinning (b).

three layers, following the definition by Carrington et al. [11]. In layer 1, which is the furthest below the contacting surface, homogeneous deformation mechanisms occur. In the case of the Stellite, this followed a sequence (with strain) of limited dislocation flow followed by mechanical twinning and then the martensitic transformation of the γ-Co to ε-Co for all test temperatures. This is in agreement with the observations of Carrington et al. [11]. Carrington [9] observed strain-induced martensitic transformation of γ-Fe (fcc) into ε-Fe (hcp) and finally α′-Fe (bct) 60 μm below the worn surface of Tristelle 5183 worn at 20 °C with a load of 40 N in lithiated water. Such transformations were not observed in this study, with diffraction patterns always indexed as γ-Fe. The deformation sequence is strongly influenced by stacking fault energy (SFE) which is strongly composition dependent, but also a function of temperature, with the SFE increasing as the temperature increases. The difference is likely to have been a difference in the manufacture route of the alloys. In the current work, the Tristelle was produced by laser cladding and so was in the as-cast condition. In contrast, Carrington [9] used HIPed material, which will be close to the equilibrium condition, which appears to have produced a matrix with lower stacking fault energy than the laser clad material. Thus, it would appear that the matrix of the Tristelle had a higher SFE than that of the Stellite.

Layer 2 is defined as the region where much higher strains are accommodated, resulting in the formation of an ultrafine grain/nanocrystalline microstructure. The transition from layer 1, with homogeneous deformation to layer 2, with more heterogeneous deformation is characteristic of low stacking fault energy materials and has been extensively reported. For example, Rainforth et al. [24] showed the deformation sequence for a 316L stainless steel, where the nanocrystalline structure was generated by the formation of shear bands in high localised strains cut through the twinned structure. Shear banding forms because the twinned or martensite plate structure limits homogeneous dislocation flow such that dislocation motion cannot accommodate the imposed strain from the contacting asperities.

The extent of layer 2 was much greater for the Tristelle than the Stellite. This again reflects the lower SFE of the Stellite compared to the Tristelle. In addition, the hard second phase particles will have played a role in the formation of layer 2. For the Stellite, the integrity of the M_7C_3 type carbides remained relatively intact, and it is believed that they play a role at homogenising the strain gradient within the matrix [11], even at the most demanding conditions and close to the surface, where they seem to flow slightly in the direction of sliding. In contrast, the carbides and silicides in the Tristelle were extensively fractured by the imposed strain. Interestingly both hard particles remained bonded to the matrix after fracture, which suggests that the flow in the matrix was relatively homogeneous.

Another important difference in the layer 2 between the two materials was the crystal structure. As noted above, no transformation was found for the Tristelle, remaining as γ-Fe up to the worn surface. In contrast, the Stellite showed complete transformation of α-Co to ε-Co for all test temperatures. Thus, the nanocrystalline layer had a hcp ε-Co structure. Moreover, locally strong textures were observed. It is known that there is easy shear along the basal planes in hcp Co, which contributes to the way Stellite is highly resistant to strain localisation, which undoubtedly reduces the depth of deformation and is also believed to contribute to the low friction (discussed earlier).

The outer layer 3 of Carrington et al.'s definition is the region containing oxide, mechanical mixing forming a complex tribofilm which is often integrated in with the nanocrystalline deformed matrix. This layer, that has already been discussed in detail, represents plastic ratcheting, with wear debris formation resulting from plastic overload and brittle fracture of the mechanically mixed layer, examples of which are extensive in the current materials, e.g. Figs. 8, 11–14. Without doubt the fracture associated with the NbC in the Tristelle has made surface delamination easier, contributing the higher wear rate of the Tristelle compared to the Stellite. Indeed, the large, brittle, NbC in the Tristelle can only be seen as a major disadvantage, compared to the relatively stable M_7C_3 in the Stellite.

5. Conclusions

1) The morphology of a surface oxide, mechanically mixed with the metal surface, determines the friction of the material. For the Stellite 6 tested at 50 N at room temperatures the friction was exceptionally high, due to stick slip behaviour of the oxide. However, as the load was increased to 200 N and above, or the temperature was increased up to 300 °C the friction decreased being the lowest for the most severe conditions of 200 N at 300 °C. This was attributed to the nature of the oxide, but also to easy shear in the strongly textured hcp ε-Co surface. In contrast, the Tristelle 5183 exhibited higher friction at all loads and temperatures (except 50 N room temperature),

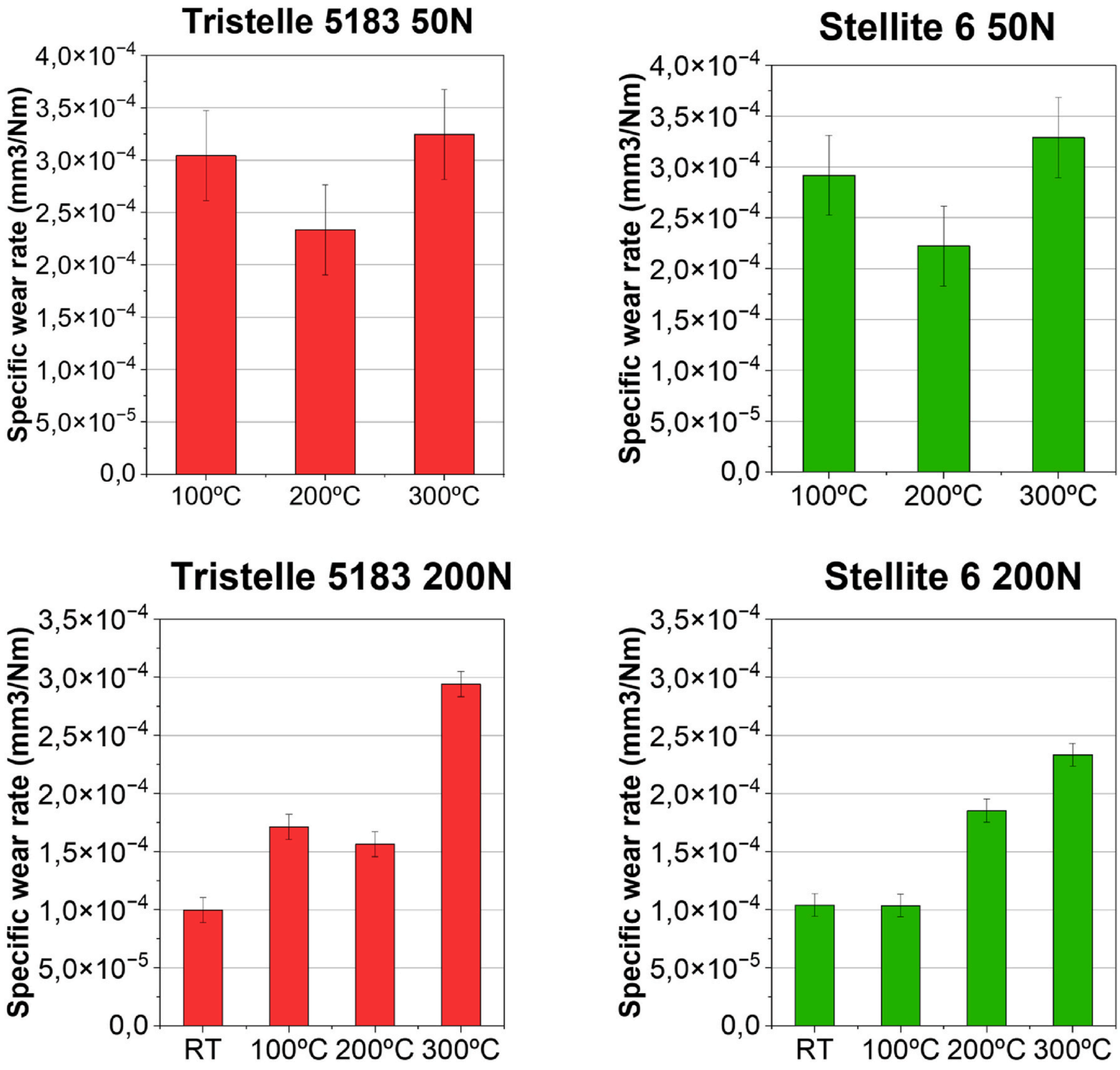

Fig. 26. Specific wear rates for each material as a function of temperature at 50 and 200 N.

attributed to the absence of easy shear at the surface and to the fragmented carbides present in the tribofilm.

2) The wear rates were not temperature sensitive for either material at a load of 50 N. This load resulted in virtually no surface deformation in Stellite and minimal deformation in the Tristelle 5183.
3) At 200 N the wear rates of both materials increased with temperature. The Stellite 6 was ~2x times more at 300 °C compared to the Tristelle 5183 which was ~3x times more at 300 °C. The more severe wear was associated with much higher degrees of surface deformation with the thickness of the deformed layer being much greater for the Tristelle 5183 than the Stellite 6.
4) The surface deformation followed the classic sequence for low stacking fault energy materials, with the formation of shear bands leading to a nanocrystalline structure in the near surface region. However, the differences in deformation mechanism between the two materials indicated that the matrix of the Stellite 6 had a lower stacking fault energy than the Tristelle 5183. This had important consequences. For the Stellite 6, transformation from fcc α-Co to hcp ε-Co well below the surface led to a nanocrystalline layer with a hcp ε-Co structure, where easy shear along the basal planes is believed to have limited damage. In contrast, no such transformation was seen for the Tristelle 5183 which remained fcc γ-Fe right up to the surface.
5) Extensive fracture of the NbC and silicide in the Tristelle 5183 was seen to a considerable depth below the worn surface. However, these hard particles were fragmented and remained adhered to the matrix, limiting the damage they will have caused. Nevertheless, this is a very unstable situation and must have had a negative impact on the wear rate and friction. In contrast, the M_7C_3 remained largely intact in the Stellite 6, thereby being able to provide load support.

Declaration of competing interest

The authors declare that they have no known competing financial interests or personal relationships that could have appeared to influence the work reported in this paper.

Acknowledgements

The funding from EPSRC (grants EP/R001766/1, EP/P02470X/1 and EP/S022635/1) and Rolls-Royce Plc is gratefully acknowledged.

References

[1] K.F. Dufrane, H. Ocken, Measurements of wear in nuclear components, Wear 101 (1985) 13–31, https://doi.org/10.1016/0043-1648(85)90209-1.
[2] R. Smith, M. Doran, D. Gandy, S. Babu, L. Wu, A.J. Ramirez, P.M. Anderson, Development of a gall-resistant stainless-steel hardfacing alloy, Mater. Des. 143 (2018) 38–48, https://doi.org/10.1016/j.matdes.2018.01.020.

[3] W.B. Burdett, Development of cobalt free wear resistant alloys for nuclear applications, Surf. Eng. 8 (1992) 131–135, https://doi.org/10.1179/sur.1992.8.2.131.

[4] G.L. Shiels, S. A, W.L. Wilson, K.W. Rosengarth, Laboratory Wire, Evaluation of low cobalt wear materials for nuclear applications, in: Third Int. Symp. Contrib. Mater. Investig. To Reduct. Probl. Encount, . Press. Water React., 1994.

[5] H. Ocken, The galling wear resistance of new iron-based hardfacing alloys: a comparison with established cobalt- and nickel-base alloys, Surf. Coating. Technol. 76–77 (1995) 456–461, https://doi.org/10.1016/0257-8972(95)02573-1.

[6] J. Vikström, Galling resistance of hardfacing alloys replacing Stellite, Wear 179 (1994) 143–146, https://doi.org/10.1016/0043-1648(94)90232-1.

[7] J.K. Kim, S.J. Kim, The temperature dependence of the wear resistance of iron-base NOREM 02 hardfacing alloy, Wear 237 (2000) 217–222, https://doi.org/10.1016/S0043-1648(99)00326-9.

[8] E.O. Olakanmi, M. Doyoyo, Laser-assisted cold-sprayed corrosion- and wear-resistant coatings: a review, J. Therm. Spray Technol. 23 (2014) 765–785, https://doi.org/10.1007/s11666-014-0098-x.

[9] M. Carrington, Microstructure Formation in the Fe-Based Hardfacing Alloy 5183 and its Sliding Wear Behaviour in High Temperature Water, PhD Thesis, University of Nottingham, UK, 2021.

[10] D. Bowden, D. Stewart, M. Preuss, Understanding the microstructural evolution of silicide-strengthened hardfacing steels, Mater. Des. 161 (2019) 1–13.

[11] M. Carrington, J.L. Daure, V.L. Ratia-Hanby, D. Zhang, P.H. Shipway, , D.A. Stewart, D.G. McCartney, Microstructural Characterisation of Subsurface Deformation and the Degradation of Stellite 6 Induced by Self-Mated Sliding Contact in a Simulated PWR Environment.

[12] J.L. Daure, M. Carrington, D.G. McCartney, D. Stewart, P.H. Shipway, Measurement of friction in galling testing – _An example of its use in characterising the galling behaviour of hardfacings at ambient and elevated temperature, Wear 476 (2021), 203736.

[13] P. Rodriguez Lago, Dry Sliding Wear Behaviour of Laser Deposited Cobalt and Iron-Based Hardfacings for Nuclear Applications, PhD Thesis, University of Sheffield, 2022.

[14] Z. Zhu, C. Ouyang, Y. Qiao, X. Zhou, Wear characteristic of stellite 6 alloy hardfacing layer by plasma arc surfacing processes, Scanning 2017 (2017) 1–7, https://doi.org/10.1155/2017/6097486.

[15] D.H.E. Persson, E. Coronel, S. Jacobson, S. Hogmark, Surface analysis of laser cladded Stellite exposed to self-mated high load dry sliding, Wear 261 (2006) 96–100.

[16] D.H.E. Persson, S. Jacobson, S. Hogmark, Antigalling and low friction properties of a laser processed Co-based material, J. Laser Appl. 15 (2003) 115–119.

[17] J. Jiang, F.H. Stott, M.M. Stack, Some frictional features associated with the sliding wear of the nickel-base alloy N80A at temperatures to 250^{o}C, Wear 176 (2) (1994) 185–194.

[18] F.H. Stott, G.C. Wood, The influence of oxides on the friction and wear of alloys, Tribol. Int. 11 (4) (1978) 211–218.

[19] J. Jiang, F.H. Stott, M.M. Stack, The role of triboparticulates in dry sliding wear, Tribol. Int. 31 (5) (1998) 245–256.

[20] H. Kato, K. Komai, Tribofilm formation and mild wear by tribo-sintering of nanometer-sized oxide particles on rubbing steel surfaces, Wear 262 (1- 2) (2007) 36–41.

[21] C. Zhao, D. Stewart, J. Jian, F.P.E. Dunne, A comparative assessment of iron and cobalt-based hard-facing alloy deformation using HR-EBSD and HR-DIC, Acta Mater. 159 (2018) 173–186.

[22] P. Crook, C.C. Li, The elevated temperature metal-to-metal wear behavior of selected hardfacing alloys, in: Wear of Materials, American Society of Mechanical Engineers, 1983, pp. 272–279.

[23] F.H. Stott, C.W. Stevenson, G.C. Wood, Friction and wear properties of Stellite 31 at temperatures from 293 to 1073 K, Met. Technol. 4 (1) (1977) 66–74.

[24] W.M. Rainforth, J. Nutting, R. Stevens, Deformation structure induced by sliding contact, Phil. Mag. 66 (4) (1992) 621–641.